Holocene fluctuations in Arctic sea-ice cover: dinocyst-based reconstructions for the eastern Chukchi Sea[1,2]

J.L. McKay, A. de Vernal, C. Hillaire-Marcel, C. Not, L. Polyak, and D. Darby

Abstract: Cores from site HLY0501-05 on the Alaskan margin in the eastern Chukchi Sea were analyzed for their geochemical (organic carbon, $\delta^{13}C_{org}$, C_{org}/N, and $CaCO_3$) and palynological (dinocyst, pollen, and spores) content to document oceanographic changes during the Holocene. The chronology of the cores was established from ^{210}Pb dating of near-surface sediments and ^{14}C dating of bivalve shells. The sediments span the last 9000 years, possibly more, but with a gap between the base of the trigger core and top of the piston core. Sedimentation rates are very high ($\sim$156 cm/ka), allowing analyses with a decadal to centennial resolution. The data suggest a shift from a dominantly terrigenous to marine input from the early to late Holocene. Dinocyst assemblages are characterized by relatively high concentrations (600–7200 cysts/cm^3) and high species diversity, allowing the use of the modern analogue technique for the reconstruction of sea-ice cover, summer temperature, and salinity. Results indicate a decrease in sea-ice cover and a corresponding, albeit much smaller, increase in summer sea-surface temperature over the past 9000 years. Superimposed on these long-term trends are millennial-scale fluctuations characterized by periods of low sea-ice and high sea-surface temperature and salinity that appear quasi-cyclic with a frequency of about one every 2500–3000 years. The results of this study clearly show that sea-ice cover in the western Arctic Ocean has varied throughout the Holocene. More importantly, there have been times when sea-ice cover was less extensive than at the end of the 20th century.

Résumé : Des carottes provenant du site HLY0501-05 sur la marge de l'Alaska dans la partie est de la mer des Tchouktches ont été analysées pour leur contenu géochimique (carbone organique, $\delta^{13}C_{org}$, C_{org}/N, $CaCO_3$) et palynologique (dinokystes, pollen, spores) afin de documenter les changements océanographiques survenus au cours de l'Holocène. La chronologie des carottes a été déterminée à partir d'une datation ^{210}Pb des sédiments près de la surface et d'une datation ^{14}C de coquilles de bivalves. Les sédiments couvrent les derniers 9000 ans, possiblement plus, mais avec une lacune entre la base de la carotte prélevée par carottier à clapet et le haut de la carotte prélevée par carottier à piston. Les taux de sédimentation sont très élevés ($\sim$156 cm/ka), permettant des analyses avec une résolution variant de décennale à centennale. Les données suggèrent un approvisionnement qui a passé de surtout terrigène à marin entre l'Holocène précoce et tardif. Les assemblages de sont caractérisés par des concentrations relativement hautes de dinokystes (600–7200 par cm^3) et une diversité élevée permettant l'utilisation d'une technique analogique moderne pour la reconstruction de la couverture des glaces de mer, des températures estivales et de la salinité. Les résultats indiquent une diminution de la couverture des glaces de mer et une augmentation, quoique bien moindre, de la température estivale de la surface de la mer au cours des 9000 dernières années. À ces tendances à long terme se superposent des fluctuations à l'échelle millénaire, caractérisées par des périodes de mince glace de mer et de températures élevées de la surface de la mer et une forte salinité qui semblent quasi cycliques, avec une période de récurrence d'une fois tous les 2500 à 3000 ans. Les résultats de cette étude démontrent clairement que la couverture des glaces de mer dans l'océan Arctique occidental a varié tout au long de l'Holocène. De manière encore plus significative, il y a eu des périodes où la couverture des glaces de mer était moins étendue qu'à la fin du 20^e siècle.

[Traduit par la Rédaction]

Received 28 April 2008. Accepted 10 September 2008. Published on the NRC Research Press Web site at cjes.nrc.ca on 30 October 2008.

Paper handled by Associate Editor P. Hollings.

J.L. McKay.[3] College of Oceanic and Atmospheric Sciences, Oregon State University, 104 COAS Admin. Building, Corvallis, OR 97331, USA.
A. de Vernal, C. Hillaire-Marcel, and C. Not. Centre GEOTOP-UQAM-McGill, Université du Québec at Montreal, CP 8888, succursale Centre-Ville, Montreal, QC H3C 3P8, Canada.
L. Polyak. Byrd Polar Research Center, Ohio State University, 1090 Carmack Rd., Columbus, OH 43210, USA.
D. Darby. Department of Ocean, Earth and Atmospheric Sciences, Old Dominion University, 4600 Elkhorn Avenue, Norfolk, VA 23529, USA.

[1]This article is one of a series of papers published in this Special Issue on the theme *Polar Climate Stability Network*.
[2]GEOTOP Publication 2008-0023.
[3]Corresponding author (e-mail: mckay_jen@yahoo.ca).

Introduction

There is clear evidence that over the last 30 years the Arctic has been experiencing dramatic environmental changes (e.g., Serreze et al. 2000; Comiso and Parkinson 2004). Most notably, there has been a rapid decline in the extent and thickness of sea-ice in summer and more recently in winter as well (e.g., Parkinson et al. 1999; Comiso 2002; Serreze et al. 2003; Rigor and Wallace 2004; Meier et al. 2005; Comiso 2006; Comiso et al. 2008; Stroeve et al. 2008). It has been suggested that if the present trend continues the Arctic could experience ice-free summers within 30 years (Stroeve et al. 2008). There is, however, debate on the relative influence of natural versus anthropogenic forcing on these recent changes. The decline in sea-ice, which began in the late 1970s, occurred contemporaneously with a major shift in Arctic atmospheric and oceanic circulation (Walsh et al. 1996), hence referred to as the Arctic Oscillation (Thompson and Wallace 1998). At this time, there was a weakening of the Arctic High that is situated over the Beaufort Sea and intensification of the Icelandic Low, conditions characteristic of the positive phase of the Arctic Oscillation (+AO). In response, the Beaufort Gyre contracted and the Transpolar Drift shifted away from Siberia to a more central position in the Arctic Ocean. The decline in Arctic sea ice associated with the +AO results primarily from the rapid removal of older, thicker ice from Arctic through Fram Strait and intensified cyclonic atmospheric circulation that brings warm air into Arctic, thus increasing sea-ice melt (Meier et al. 2005). However, sea ice has continued its rapid decline, since the AO returned to a more neutral state in the late 1990s, suggesting that anthropogenic warming of surface air temperatures is playing a role in the loss (Overland and Wang 2005), as now recognized by the Intergovernmental Panel on Climate Change (IPCC 2007).

The primary objective of this paper is to investigate the natural variability of sea-ice cover in the western Arctic during the Holocene and thus provide a baseline to which recent changes can be compared. Sea-ice cover, as well as summer sea-surface temperature (SST) and salinity (SSS), for the Holocene are quantitatively reconstructed by applying the modern analogue technique to dinocyst assemblages (de Vernal and Hillaire-Marcel 2000; de Vernal et al. 2001, 2005*b*). Dinocysts are organic-walled cysts of dinoflagellates that protect the diploid cell after sexual reproduction (e.g., Head 1996). They are a particularly useful proxy in the Arctic Ocean because the assemblages are characterized by a relatively high diversity of species and they are generally well preserved compared with calcareous and siliceous microfossils (de Vernal et al. 2001; Mudie et al. 2001). More importantly, in the Arctic Ocean and subarctic seas, dinocyst assemblages are highly sensitive to sea-surface conditions, including temperature, salinity, and sea-ice cover (Kunz-Pirrung 2001; Mudie and Rochon 2001; Radi et al. 2001; Voronina et al. 2001; de Vernal et al. 2001, 2005*b*; Matthiessen et al. 2005).

The study area is located on the eastern Chukchi slope (415 m water depth; 72.69°N, 157.52°W), west of Point Barrow, Alaska (site HLY0501-05, Fig. 1). This region of the western Arctic experiences changes in surface ocean circulation related to the AO. During periods of anticyclonic circulation (i.e., –AO) the Beaufort Gyre expands and influences surface circulation in the region; whereas during periods of cyclonic circulation (+AO) the Beaufort Gyre contracts and the Transpolar Drift crosses the study area (Fig. 1). These changes in circulation in turn influence sea-ice drift and thus ice export from the Arctic (e.g., more rapid removal of sea-ice during +AO; Steele and Boyd 1998; Kwok 2000). Ice-drift records for the Holocene, which identify sea-ice source based on the composition of iron oxide grains, suggest millennial-scale change in the source of sea ice that is interpreted as a response to shifts in the location of the Transpolar Drift, akin to changes that occur during different phases of the AO (Darby et al. 2001; Darby and Bischof 2004). Paleoceanographic studies also indicate that sea-ice cover in the western Arctic has varied throughout the Holocene (de Vernal et al. 2005*a*, 2008; Ledu et al. 2008). However, due to the low chronological resolution of the data, millennial and higher frequency changes could not be unequivocally identified. This study was initiated to investigate Holocene variations in sea-surface conditions, notably sea-ice cover, at a much higher temporal resolution. This is now possible because of the existence of new sediment cores collected during the 2005 HOTRAX expedition (Darby et al. 2005).

Hydrography of the western Arctic

The water column structure of the Arctic Ocean is characterized by a cold, low-salinity mixed layer (0–30 m), a strong halocline characterized by an inverse thermocline (30–200 m), a relatively warm Atlantic water layer (200–800 m), and below ~800 m, a number of deep-water masses. The low-salinity surface layer is the result of riverine input of freshwater as well as sea-ice melting in summer (Aagaard et al. 1981). In the western Arctic, subsurface waters within the halocline consist of a mixture of brines released during sea-ice formation and water originating from the Pacific and Atlantic oceans. The flux and temperature of Atlantic water flowing into the Arctic Ocean appear to correlate with fluctuations in the Arctic and North Atlantic oscillations (AO and NAO, respectively), with a higher input of relatively warm Atlantic water entering through Fram Strait and the Barents Sea during positive phases of the AO and NAO (McLaughlin et al. 1996; Grotefendt et al. 1998; Morison et al. 1998; Dickson et al. 2000). Changes in Atlantic water influx also seem to have occurred on much longer timescales. For example, Atlantic water inflow appears to have been relatively high during the early Holocene (Polyak and Mikhailov 1996; Duplessy et al. 2001; Voronina et al. 2001; Sarnthein et al. 2003; Andrews and Dunhill 2004; Hillaire-Marcel et al. 2004; de Vernal et al. 2005*a*; Duplessy et al. 2005; Slubowska et al. 2005).

Materials and methods

During leg 1 of the 2005 HOTRAX expedition (Darby et al. 2005), sediment cores were collected from the Alaska margin, west of Point Barrow (i.e., eastern Chukchi shelf and slope). In this paper, we discuss results for a 16.73 m long piston core and the corresponding 2.59 m long trigger core that were collected from a water depth of 415 m (site HLY0501-05, Fig. 1). The trigger core and upper 12.4 m of the piston core are composed of a sulphide-rich, olive-gray

Fig. 1. Map of the Arctic, showing the location of site HLY0501-05 (see inset) and surface flows associated with the Beaufort Gyre and Transpolar Drift (Arctic map modified from Dyke et al. 1997 and reference therein).

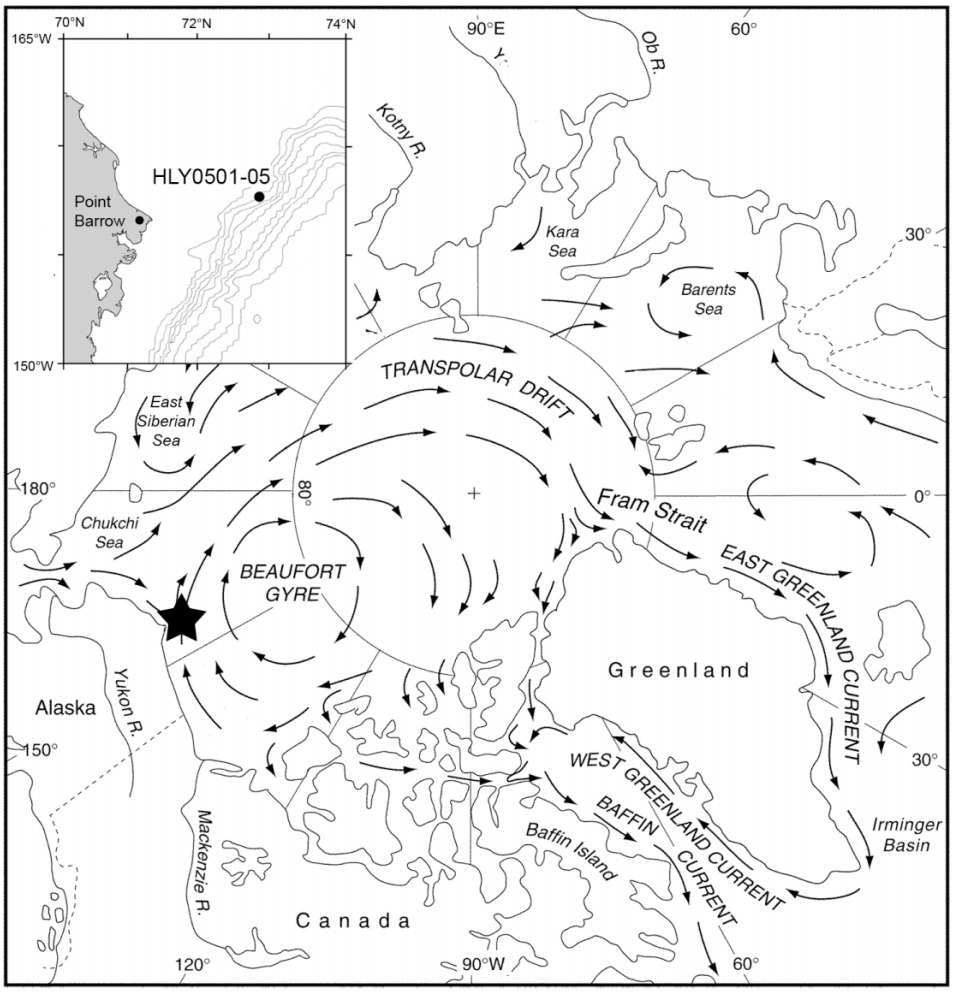

Table 1. Radiocarbon data for piston core HLY0501-05.

Sample	Composite depth (cm)	Corrected depth (cm)	Sample type	Uncorrected ^{14}C age (years)	Calendar age (years BP) $\Delta R = 0$	CAMS No.[b]
Section 1, 36–38 cm	36.0–38.0	112.0	Bivalve, Thyasira	1930±45	1468	128414
Section 4, 76–78 cm	483.0–485.0	559.0	Bivalve, Yoldia	4465±40	4572	128415
Section 5, 12–14 cm	568.5–570.5	644.5	Bivalve, Thyasira	4820±70	5130	128416
Section 5, 132–134 cm	688.5–690.5	764.5	Bivalve, Yoldia	5220±40	5593	128417
Section 6, 88–90 cm	799.0–801.0	875.0	Bivalve, Portlandia[a]	5885±40	6306	128418
Section 7, 18–20 cm	879.5–881.5	955.5	Bivalve, Portlandia and Thyasira[a]	6395±45	6867	128419

[a]CAMS, Center for Accelerator Mass Spectrometry; measured at the Lawrence Livermore National Laboratory, University of California, Livermore, California.

[b]Portlandia sp. are deposit feeders and may incorporate old organic matter and thus maybe artificially old (Forman and Polyak, 1997).

mud (unit 1). In the piston core, unit 1 is underlain by 4.33 m of gray to gray-brown sandy mud that contains abundant ice-rafted debris (unit 2).

The age model for unit 1 is based on six accelerator mass spectrometry (AMS) radiocarbon dates of bivalve shells collected from the piston core (Table 1). Radiocarbon dates were converted to calendar ages using CALIB version 5.0.2 (Stuiver et al. 2005), assuming a reservoir age of 400 years and a regional reservoir correction (ΔR) of 0 years. A zero ΔR was employed because the coring site is overlain by relatively young Atlantic water (average ΔR = 75 years in the Kara and Barents seas; Forman and Polyak 1997) and is situated well below the halocline (30–200 m) and thus not influenced by older Pacific water that is characterized by a much larger ΔR (i.e., 460 years based on radiocarbon data from McNeely et al. 2006). The use of a small ΔR is also supported by a comparison of paleomagnetic data for piston core HLY0501-05 with other well-dated Northern Hemi-

Fig. 2. (*a*) Uncorrected ^{14}C age versus corrected piston core depth. The horizontal broken line marks the contact between units 1 and 2. (*b*) $Ln^{210}Pb$ versus trigger core depth. The zone from 4.5 to 8.0 cm (open triangles) may represent a period of very intense bioturbation or possibly very rapid deposition, although there is no visible change in the character of the sediment.

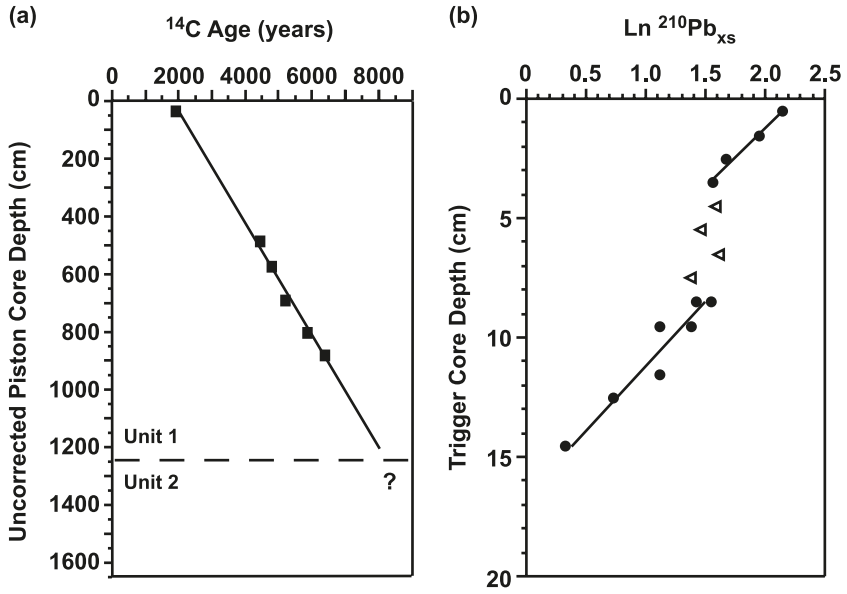

sphere paleomagnetic records (Barletta et al. 2008). Radiocarbon dating of unit 1 suggests an average sedimentation rate of about 156 cm/ka (Fig. 2*a*), which is similar to the sedimentation rates estimated from ^{210}Pb measurements of the trigger core (average 160.5 cm/ka; Fig. 2*b*). Based on dating, it appears that >1 m of sediment was lost off the top of the piston core during its collection. Moreover, substantial differences in the palynological assemblage of the upper 100 cm of the trigger core and the top of the piston core, presented in this paper, also indicate no overlap. Composite data records are, therefore, presented versus age based on sedimentation rates mentioned earlier (trigger core = 160 cm/ka; unit 1 of the piston core = 156 cm/ka) and assuming that the trigger core includes the surface sediment and that sediment accumulated over the last 1400 years is missing from the piston core. This results in a time gap of ~700 years between the base of section 1 of the trigger core and the top of the piston core.

Geochemical (i.e., organic carbon, calcium carbonate, and total nitrogen) and grain-size (i.e., >106 μm) measurements were made every 8 cm, which yields a resolution of ~50 years between samples. Total carbon and total nitrogen contents were measured using a Carlo Erba NA2500 elemental analyzer. The error, which is based on replicate analyses for each sample, is generally better than ±0.008% for C and ±0.003% for N. The inorganic carbon concentration was measured using a UIC Coulometer and has a standard deviation (1σ) of 1.5% based on the repeated analysis of a $CaCO_3$ standard. The percent organic carbon (C_{org}) was calculated by difference (C_{org} = total C – inorganic C). The carbon isotopic composition of organic matter ($\delta^{13}C_{org}$) was measured by continuous-flow mass spectrometry using a Carlo Erba elemental analyzer connected to an Isoprime mass spectrometer. Results are presented in the standard δ notation versus VPDB. A precision of ±0.05‰ is estimated based on replicate analyses of selected samples.

Palynological analyses were made at an 8 cm sampling interval for the trigger core and upper 3.5 m of the piston core, which yields a resolution of ~50 years between samples. Below 3.5 m, the sampling interval was about 24 cm, yielding a resolution of ~150 years between samples. Samples for palynological analysis were prepared following the standard procedure of the micropaleontological laboratory at Centre GEOTOP, Montréal, Quebec (de Vernal et al. 1996). In brief, samples were wet sieved at 10 and 106 μm to remove the fine silt and clay and the coarse sand, respectively. The 10–106 μm size fraction was treated several times with HCl (10%) and concentrated HF to dissolve carbonate and silica particles, respectively. The remaining residue was mounted in glycerin gel for observation in transmitted light microscopy at 400× to 1000× magnification. A minimum of 200 dinocyst specimens were counted and identified in each sample following the taxonomy in Matthiessen et al. (2005). Pollen grains, spores, and reworked palynomorphs of pre-Quaternary age were also counted. The concentration of palynomorphs was calculated from the marker-grain method (Matthews 1969) by the addition of *Lycopodium* tablets. This method provides results with a reproducibility of ~10% for a 0.95 confidence interval (de Vernal et al. 1987).

Herein, we utilize total concentrations of pollen grains and reworked palynomorphs as tracers of allochthonous inputs from the adjacent landmass (terrestrial vegetation and erosion of surrounding outcrops, respectively; cf. de Vernal and Marret 2007). In comparison, dinocysts relate to pelagic production in surface waters. Their assemblages permit the reconstruction of sea-surface conditions (summer salinity, summer temperature, and number of months/year with >50% sea-ice cover). Reconstructions were made using the modern analogue technique (MAT) and the 3Pbase software of Guiot and Goeury (1996). MAT is a method based on similarities between modern and fossil species assemblages. It is one of the most reliable methods among transfer functions sensu lato that allows the simultaneous reconstruc-

Fig. 3. (*a*) Downcore profiles of organic carbon (circles) and carbonate (triangles). (*b*) Downcore profiles of the organic carbon to total nitrogen ratio (C_{org}/N, diamonds) and the carbon isotopic composition of organic matter ($\delta^{13}C_{org}$, squares). Trigger core (Tc) data are shown by the solid symbols and piston core (Pc) data by the open symbols.

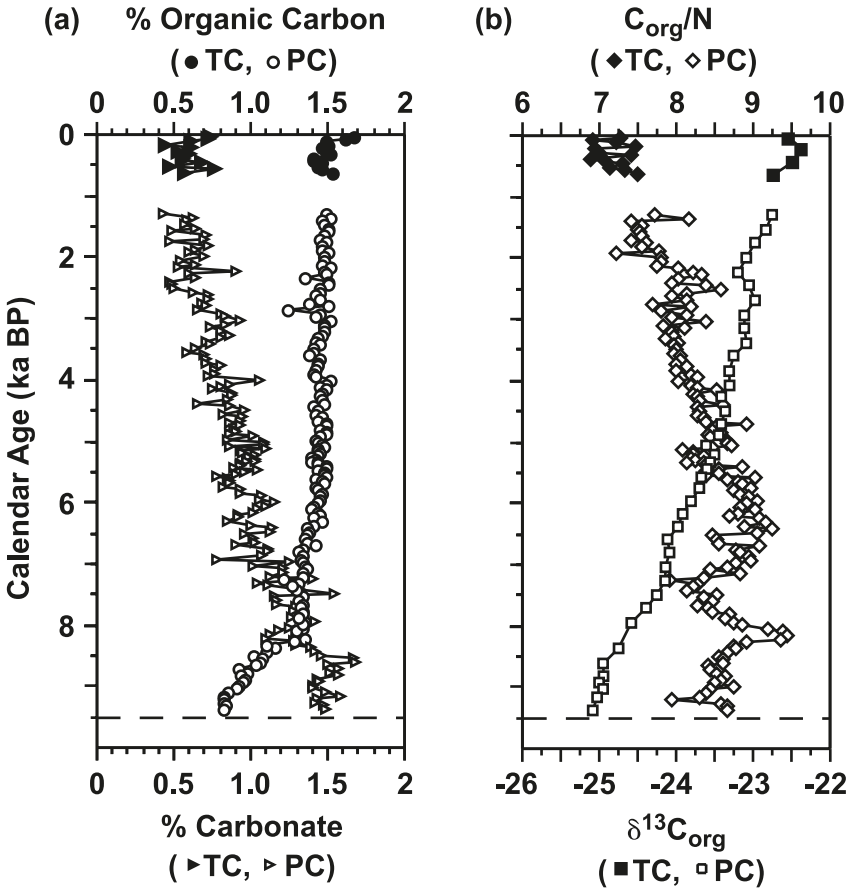

tion of several parameters (Guiot and de Vernal 2007). MAT was applied to dinocyst assemblages following the procedures described in de Vernal et al. (2005*b*). We used a reference dinocyst database that includes 64 taxa and 1089 reference sites from the mid- to high-latitude North Atlantic, North Pacific, and Arctic oceans and adjacent sub-polar seas (updated from Radi and de Vernal 2008). Hydrographic estimates were calculated from a set of five modern analogues selected from the reference database after logarithmic transformation of the relative abundances of taxa. The hydrographic data were compiled for a radius of 30 nautical miles around each reference site using the 2001 version of the World Ocean Atlas (www.nodc.noaa.gov/OC5/WOA01/woa01dat.html). At many sites in the Arctic and subarctic seas, however, hydrographic data and especially salinity data are very rare, which introduce some uncertainties in reconstructions. Sea-ice cover data were compiled at 1° by 1° grid scale from the 1953–2000 dataset provided by the National Snow and Ice Data Center (NSIDC) in Boulder, Colorado (nsidc.org/data/docs/noaa/g00799_arctic_southern_sea_ice/). Sea-ice cover is expressed here in terms of months per year with a sea-ice concentration >50%. It is a parameter that correlates with the mean annual sea-ice concentration (cf. de Vernal et al. 2005*a*). The overall error of prediction calculated from modern assemblages is ±1.5 °C for the summer SST, ±1.8 for the summer salinity in the >20 salinity domain, and ±1.1 months/year of sea ice.

Results

Geochemical data are provided in Appendix A (Table A1). The organic carbon content of the sediments increased rapidly from 0.80% to 1.30% between 9500 and 8300 years BP (Fig. 3*a*). Over the past 8300 years, the organic carbon concentration has slightly increased up to 1.60% in surface sediments (Fig. 3*a*). In comparison, the carbonate content has slowly decreased from 1.5% to 0.6% throughout the Holocene (Fig. 3*a*). The C_{org}/N ratios fluctuated between 8.0 and 9.5 in the early Holocene, prior to 6500 years BP, and then slowly decreased to about 7.0 in the late Holocene (Fig. 3*b*). The $\delta^{13}C_{org}$ values have steadily increased throughout the Holocene, from –25.0‰ to –23.5‰ in the youngest sediments (Fig. 3*b*). Pollen concentrations have decreased continuously throughout the Holocene (Fig. 4*a*).

The concentrations of reworked palynomorphs and coarse-grained (>106 μm) material are very high in unit 2 (>500 cm^3 and >2%, respectively) and then decrease sharply at the contact between units 1 and 2 (Figs. 4*b*, 4*c*). Concentrations of these materials are generally low throughout unit 1, although there is a zone of slightly higher values near the base (prior to 7300 years BP, Figs. 4*b*, 4*c*). The contact between units 1 and 2 represents a significant change in the character of sedimentation on the Alaska margin. The date of the transition is certainly >7000 years and is estimated at ~9500 years BP based on the linear extrap-

Fig. 4. Down core concentrations of (*a*) pollen, (*b*) reworked material, (*c*) coarse-grained material (i.e., >106 μm size fraction), and (*d*) dinocysts. The horizontal broken line indicates the contact between units 1 and 2. Trigger core (Tc) data are shown by the solid symbols and piston core (Pc) data by the open symbols. cc, cm^3.

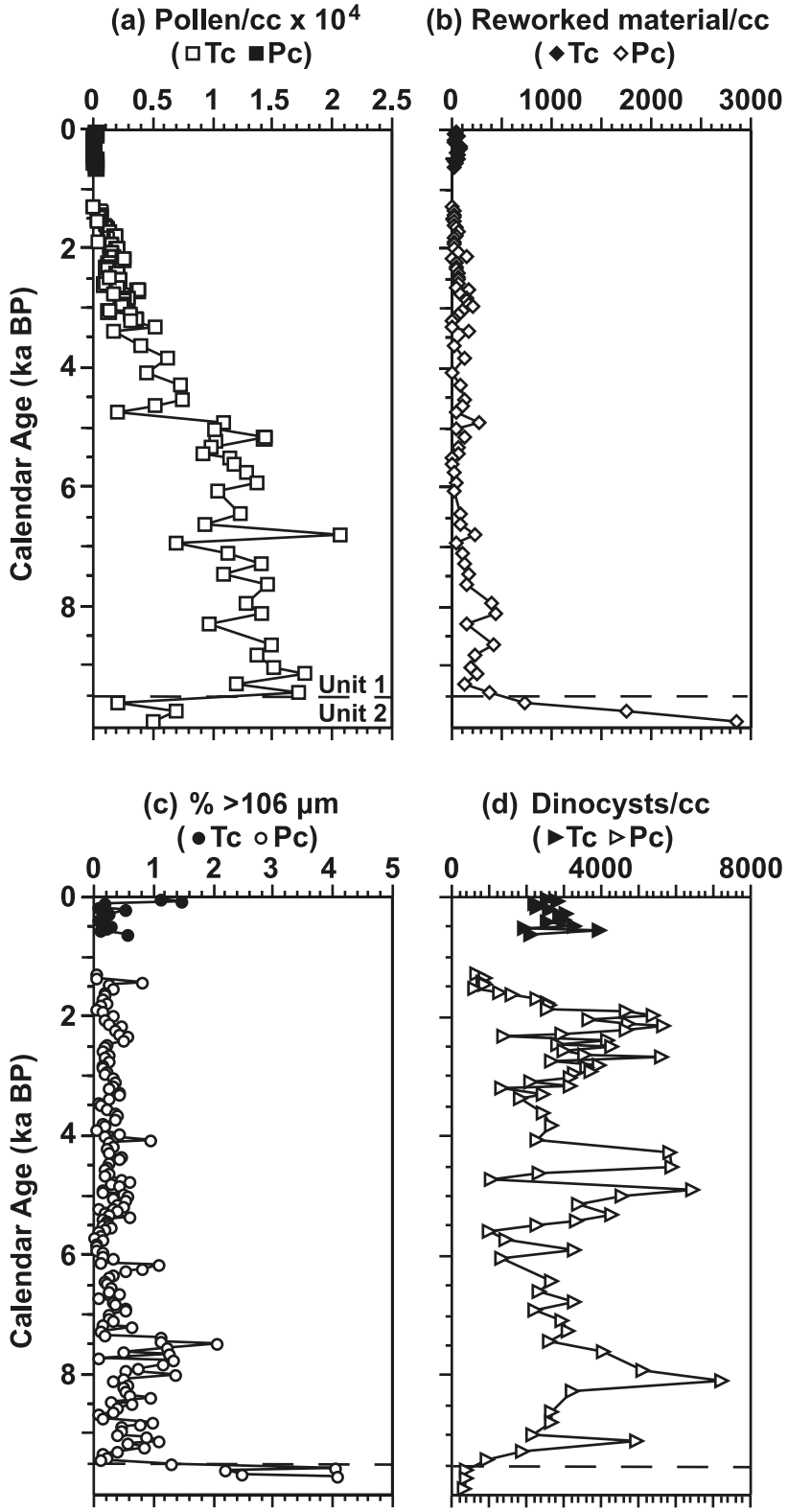

olation of ^{14}C ages versus depth (Fig. 2). The possible cause(s) behind this change are currently being investigated.

Dinocyst assemblage data are provided in Appendix A (Table A2). Concentrations in unit 1 range from 600 to 7200 cysts/cm^3 (Fig. 4*d*). Such values correspond to fluxes on the order of 10–100 cysts/cm^2/year, which indicate rela-

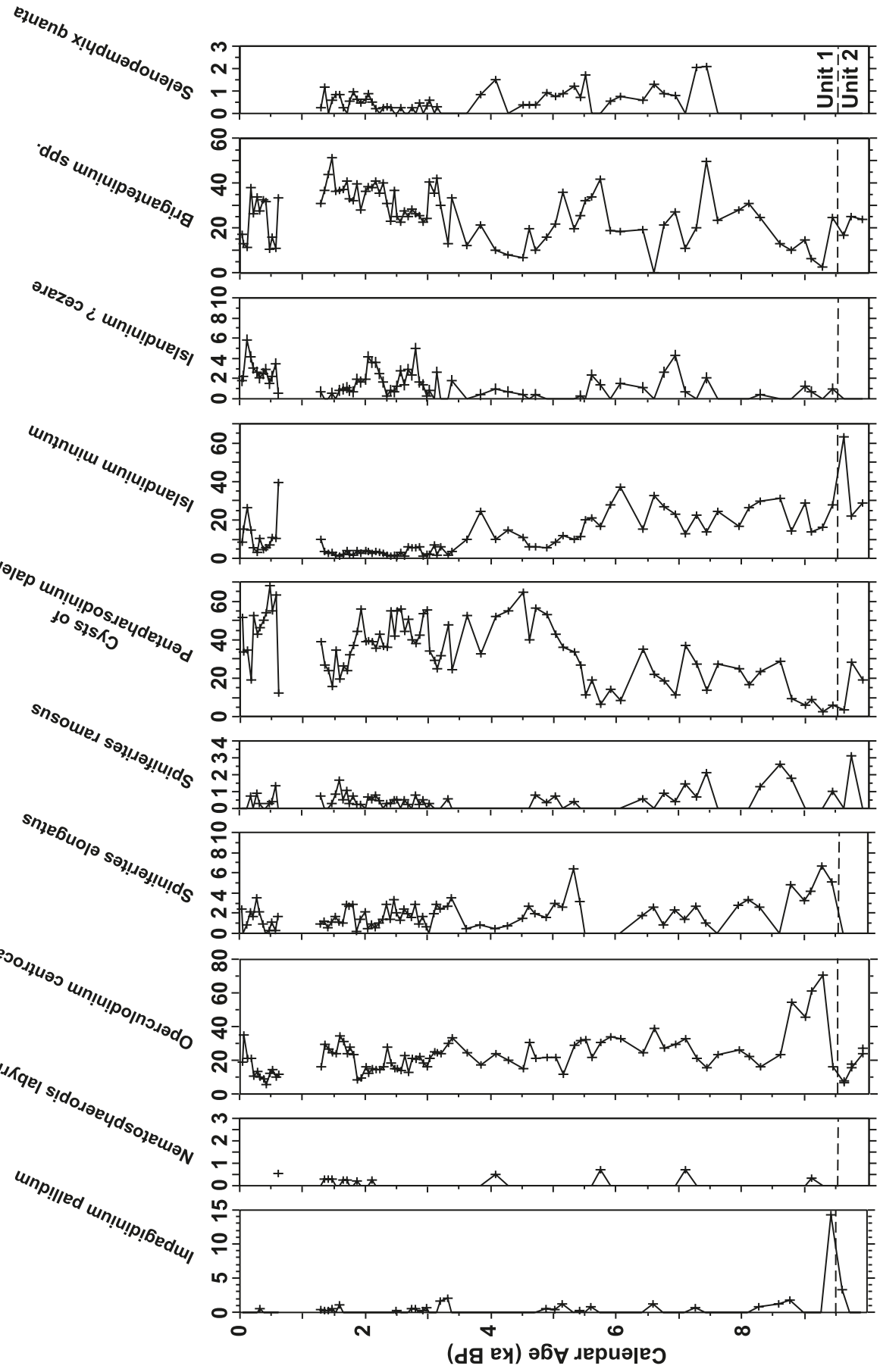

Fig. 5. Percentages of dinocyst taxa in the trigger core (down to ca. 600 years BP) and piston core (ca. 1300–9500 years BP) from site HLY0501-05. The horizontal broken line indicates the contact between units 1 and 2.

Fig. 6. Relationship between the percentages of *Pentapharsodinium dalei* and *Islandinium minutum* and (*a*) summer sea-surface temperature and (*b*) sea-ice cover at the 1189 modern sites in the reference dinocyst database.

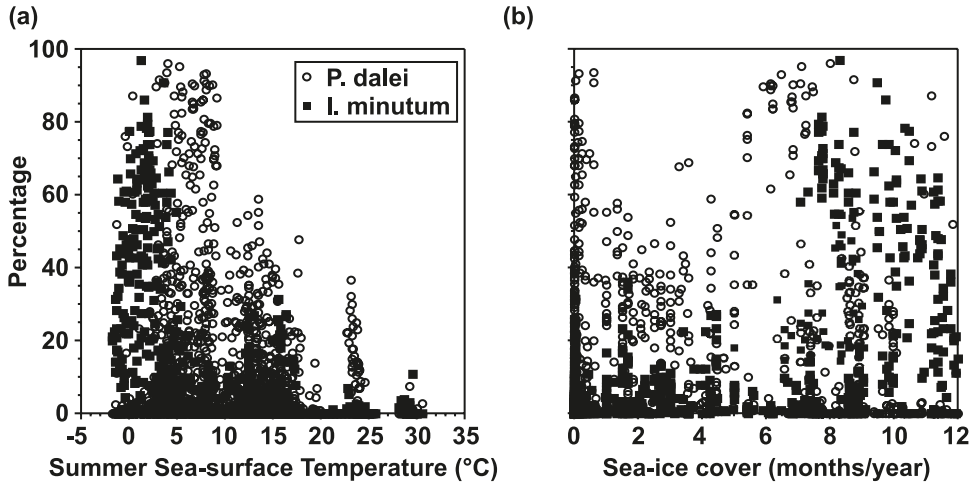

Fig. 7. Reconstructions of Holocene (*a*) sea-ice cover, (*b*) summer sea-surface salinity (SSS), and (*c*) summer sea-surface temperature (SST) for cores from site HLY0501-05. Trigger core data are shown by the solid symbols and piston core data by the open symbols. The thick line is the data smoothed using a 5-point average. Modern sea surface conditions are shown by the thick bar on the *x* axis (modern range). The shaded zones indicate times of relatively low sea ice, higher summer SSS, and high SST. The overall error of prediction calculated from modern assemblages is ±1.5 °C for the summer SSTs, ±1.8 for the summer salinity in the >20 salinity domain, and ±1.1 months/year of sea ice.

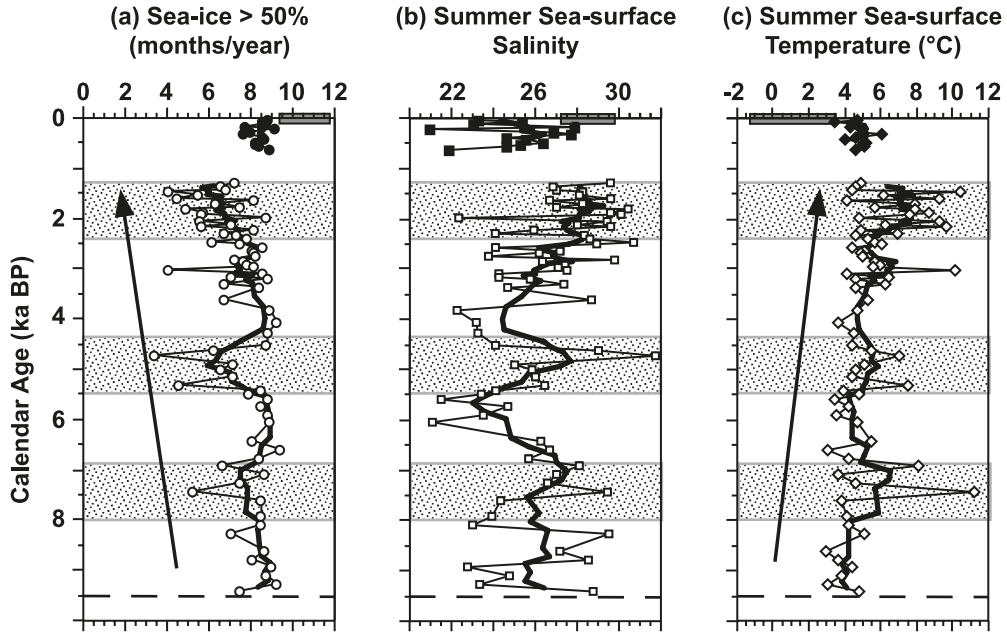

tively high productivity (e.g., de Vernal et al. 1994). The relative abundances of the most common dinocysts taxa in core HLY0501-05 are shown in Fig. 5. The dominant taxa, composing >90% of the total assemblage, are *Pentapharsodinium dalei*, *Brigantedinium* spp., *Operculodinium centrocarpum*, and *Islandinium minutum*. Such taxa are common in the modern Chukchi Sea (Radi et al. 2001), the Arctic Ocean, and subarctic seas in general (e.g., de Vernal et al. 2001; Mudie and Rochon 2001; Matthiessen et al. 2005). The changes in relative abundance of these taxa nevertheless suggest variations in sea-surface conditions throughout the Holocene. In particular, the increase of *P. dalei* relative to the decrease of *I. minutum* at about 5500 years BP may reflect a warming in surface waters, as suggested by the modern distribution of both taxa (Fig. 6). There are also variations in the occurrence of minor taxa such as *Nematosphaeropsis labyrinthus*, *Impagidinium pallidum*, *Selenopemphix quanta*, *Spiniferites elongatus*, and *Spiniferites ramosus*. Because these taxa have narrower ecological affinities for subpolar to temperate conditions, peaks in their occurrence may suggest relatively warm periods.

Holocene sea-surface conditions at site HLY0501-05 were reconstructed using MAT as indicated in the method section. Most of the modern analogue sites that were selected during

this process are located in the Arctic (e.g., 36.4% from Beaufort Sea, 30.4% from Hudson Bay, 15.5% from eastern Arctic Ocean, and 4.8% from Bering Sea). The reconstructions of SST, SSS, and sea-ice cover are shown in Fig. 7. The reconstruction for the trigger core covers the last 600 years. According to sea-surface temperature estimates, the last few hundred years have been marked by cooler conditions than most of the Holocene, with summer SST values of ~4 °C and extensive sea-ice cover spanning ~9 months/year. The overall record for the piston core is marked by a long-term Holocene trend of increasing summer SST from about +3 °C prior to 7000 years BP to +7 °C ~2000 years BP. This trend is accompanied by decreasing sea-ice extent from 9 to 6 months/year. Superimposed on these long-term trends are millennial-scale fluctuations in sea-surface conditions marked by periods of minimum sea ice (below modern values) and corresponding maxima in summer SSS and SST (similar to or higher than modern values). These fluctuations appear quasi-cyclic with episodes of reduced sea-ice cover centered at about 7500, 5000, and 2000 years BP, yielding a frequency of ~1 every 2500–3000 years. It is also apparent that the amplitude of sea-ice fluctuations has increased from early to late Holocene owing to a progressive decrease in the minimum sea-ice values.

Discussion

The 1.5‰ increase in $\delta^{13}C_{org}$ values from the early to late Holocene reflects decreasing terrestrial organic matter input relative to marine fluxes, which is consistent with the decrease in C_{org}/N ratios (Fig. 3*b*) and also the decrease in pollen concentrations (Fig. 4*a*). A similar decrease in the terrestrial organic matter content of sediments following the last glacial maximum has been documented in both the Laptev Sea (Mueller-Lupp et al. 2000) and the Kara Sea (Kang et al. 2007). This decrease in terrestrial organic matter flux to the Arctic seas during the early Holocene can be attributed to a landward shift in the sites of terrestrial organic matter deposition associated with rising sea level (e.g., Mueller-Lupp et al. 2000). Flooding of the Chukchi shelf and opening of the Bering Strait occurred at ca. 12 000 years BP (Keigwin et al. 2006) and sea level reached close to the modern height by ca. 7000 years BP (Mueller-Lupp et al. 2000; Mason and Jordan 2002), with a slight rise of ~1.5 m over the last 6000 years (Mason and Jordan 2002). The continual decrease in terrestrial content in the mid- to late Holocene sediments of core HLY0501-05 could reflect a reduction in the terrestrial organic material reworked from the peatlands of the Bering Land Bridge including the Chukchi shelf and Alaska coastline that were inundated during the postglacial times (e.g., Jordan and Mason 1999; Jordan 2001). Alternatively, a decrease in the amount of terrestrial organic matter transported westward from the Mackenzie River by the Beaufort Gyre could be invoked in relation to a strengthening of the Mackenzie Current, an eastward flowing coastal current that today carries material toward the Canadian Arctic Archipelago. This interpretation is consistent with driftwood records from the region. The absence of driftwood on Victoria Island prior to ~4700 years BP and the progressive increase in driftwood occurrence after this time have been cited as evidence of a strengthening Mackenzie Current from the mid- to late Holocene (Dyke and Savelle 2000). Although it is possible that the northward migration of the treeline, as recorded in the Keewatin and Labrador regions since the mid-Holocene (Bigelow et al. 2003), could also explain the driftwood record. The identification of the source of terrestrial organic matter found in core HLY0501-05 would be indispensable for an unequivocal interpretation.

Modern sea-ice cover in the study area, expressed here as the number of months/year with >50% coverage, averages 10.6 ± 1.2 months/year (cf. 1954–2001 data from NSIDC; nsidc.org/data/docs/noaa/g00799_arctic_southern_sea_ice/). Present-day SST and SSS in August are 1.1 ± 2.4 °C and 28.5 ± 1.3, respectively (NODC 2001 World Ocean Atlas; www.nodc.noaa.gov/OC5/WOA01/woa01dat.html). In the Holocene record of core HLY0501-05, sea-ice cover has ranged between 5.5 and 9 months/year, summer SSS has varied between 22 and 30, and summer SST has ranged from 3 to 7.5 °C (Fig. 7). The reconstructions, even at the top of the trigger core, seem to yield milder conditions than those given for the site by the World Ocean Atlas. Some of this difference may be due to the uncertainties in the hydrographical data that are very limited in the Arctic. It can also be related to the inherent errors associated with the transfer function method. The hydrographical estimates at the top of the trigger core are compatible with modern averages when taking into account the standard deviation of observations and the error of prediction (RMSE) calculated from validation exercises (see Method section). In any case, because the database includes many sites from the Arctic Ocean and the Beaufort Sea in particular, we cannot attribute the difference to a bias linked to limited analogues at the cold end of the database. Furthermore, given the high dinocyst fluxes at the coring site and the fact that the location is remote from warmer oceans, it is unlikely that the assemblages are affected by the addition of cysts transported over a long distance. In fact, the assemblages in the study cores clearly relate to periods of high productivity and the high species diversity reflect mild conditions relative to the cold end of the database. The difference between the top of the sequence and the "modern" hydrography might well be due to the fact that the top of the trigger core represents a longer time interval than that of the limited numbers of hydrographic measurements, which were made between 1954 and 2001. If both the observed and reconstructed time series are correct, then the last part of the 20th century must have been particularly cold compared with the mid- to late Holocene in the Chukchi Sea, which is opposite to what is seen in the eastern Arctic and northern Baffin Bay (e.g., de Vernal et al. 2008). This hypothesis implies a strong regionalism in climate changes over the Arctic and deserves to be further explored because it has some important implications with regard to the significance of the "modern" climatology in the Arctic.

Nevertheless, the dinocyst reconstructions for site HLY0501-05 clearly show that sea-surface conditions, notably sea-ice cover, have fluctuated significantly during the Holocene. Since the early Holocene, sea-ice cover exhibits a general decreasing trend. This is in direct contrast to the eastern Arctic where sea-ice cover was substantially reduced during the early to mid-Holocene and has increased over the

last 3000 years (Dyke et al. 1996; Dyke et al. 1997; Levac et al. 2001; Mudie et al. 2006; Rochon et al. 2006). Superimposed on these long-term changes are millennial-scale variations that appear to be quasi-cyclic, with minima in sea-ice cover and corresponding maxima in summer SSS and SST occurring about every 2500–3000 years. This type of cyclicity may be associated with regional climate changes. One possible mechanism is related to changes in freshwater input, which influences stratification, and thus vertical mixing of surface water with underlying warm, saline Atlantic water. Increased mixing would result in higher salinity and inhibit sea-ice formation, thus enhancing heat accumulation in the surface water during spring and summer. Decreases in freshwater inputs from Russian Arctic rivers, for example, may contribute to reduced stratification and decreased sea-ice formation. The influx of relatively fresh Pacific water via the Bering Strait may have also played an important role in the strength of the halocline in the western Arctic, as it does today. Alternatively, more intense vertical mixing in the upper water column due to particularly strong winds and (or) tidal amplification (e.g., Keeling and Whorf 1997) may have influenced stratification. Whatever the underlying mechanism(s), changes in vertical stratification must be considered as a key parameter in Arctic sea-ice coverage. Thus, we suggest that the episodes of reduced sea-ice cover and corresponding relatively high sea-surface salinity and temperature that are centered at ~7500, 5000, and 2000 years BP (shade zones, Fig. 7) might correspond to episodes of stronger vertical mixing in the upper water column.

Arctic marine records for the Holocene are rare but those that are available, for example from the Beaufort Sea and Lancaster Sound – northern Baffin Bay (e.g., Rochon et al. 2006; Ledu et al. 2008), do exhibit millennial-scale cyclicity. In the northern North Atlantic and Nordic seas, millennial cycles are also reported with spectral periodicity that generally ranges from 800 to 1500 years (e.g., Bond et al. 1997, 2001; Klitgaard-Kristensen et al. 2001; Calvo et al. 2002; Sarnthein et al. 2003). The Holocene ice core records of Greenland also exhibit millennial-scale variability at periodicities varying from 510 to 2600 years (e.g., O'Brien et al. 1995; Grootes and Stuiver 1997; Schulz and Paul 2002; Mayewski et al. 2004). Millennial-scale oscillations thus seem to be an important feature of the high-latitude climate system, but the actual periodicity (or periodicities) are equivocal and different forcing mechanisms are most probably involved (for a synthesis, see Paul and Schulz 2002). It is possible that millennial-scale oscillations of sea-surface conditions in the western Arctic is an amplified response to changes in incoming solar radiation, given that it has a similar periodicity as a Holocene cycle observed in the Greenland Ice Sheet Project 2 (GISP2) ice core (Grootes and Stuiver 1997). It is also possible that tidal forcing plays a major role, since it intensifies vertical mixing in the water column. In the Nordic seas, such a mechanism linked to lunar forcing seems also to have affected regional sea ice (cf. Yndestad 2006) and may do so in the Arctic Ocean as well. Lastly, variable contribution of Pacific water entering the Arctic Ocean through the Bering Strait must be considered, especially as it is influenced by the AO (Steele et al. 2004). Clearly, further work is needed to document the millennial nature of hydrographical changes in the western Arctic and better understand the causes and mechanisms involved.

Conclusion

The Holocene record from site HLY0501-05 illustrates the sensitivity of hydrographical conditions in the western Arctic Ocean. The data show a long-term warming that is opposite to what is reconstructed for the eastern Arctic and point to a bipolar behavior of the Arctic Ocean at the timescale of the Holocene. The millennial-scale variability in the eastern Chukchi Sea is characterized by quasi-cyclic periods of high SSS, high SST, and reduced sea-ice cover, which most probably reflects variations in the stratification of the upper water column. Such changes maybe related to tidal forcing and (or) large-scale mechanisms, such as AO/NAO-like oscillations. It is important to note that the amplitude of these millennial-scale changes in sea-surface conditions far exceed those observed at the end of the 20th century.

Acknowledgements

The authors would like to thank two anonymous reviewers for their constructive comments as well as the editorial staff at CJES. This study is a contribution to the Polar Climate Stability Network (PCSN) supported by the Canadian Foundation for Climate and Atmospheric Sciences (CFCAS). Complementary support was provided by the Natural Sciences and Engineering Research Council (NSERC) of Canada and the Fonds Québécois de la Recherche sur la Nature et les Technologies (FQRNT) of Québec. The HOTRAX 2005 coring expeditions was supported by a US National Science Foundation (NSF) award to D. Darby and L. Polyak (OPP-9817051/98170540). This paper is dedicated to the memory of Maxime Paiement.

References

Aagaard, K., Coachman, L.K., and Carmack, E. 1981. On the halocline in the Arctic Ocean. Deep-Sea Research, **28**: 529–545. doi:10.1016/0198-0149(81)90115-1.

Andrews, J.T., and Dunhill, G. 2004. Early to mid-Holocene Atlantic water influx and deglacial meltwater events, Beaufort Sea slope, Arctic Ocean. Quaternary Research, **61**: 14–21. doi:10.1016/j.yqres.2003.08.003.

Barletta, F., St-Onge, G., Channell, J.E.T., Polyak, L., and Darby, D.A. 2008. High-resolution paleomagnetic secular variations and relative paleointensity records from the western Canadian Arctic: implications for Holocene stratigraphy and geomagnetic field behaviour. Canadian Journal of Earth Sciences, **45**: this issue.

Bigelow, N.H., Brubaker, L.B., Edwards, M.E., Harrison, S.P., Prentice, I.C., Anderson, P.M., et al. 2003. Climate change and Arctic ecosystems: 1. Vegetation changes north of 55°N between the last glacial maximum, mid-Holocene, and present. Journal of Geophysical Research, **108**: No. 8170. doi:10.1029/2002JD002558.

Bond, G., Showers, W., Cheseby, M., Lotti, R., Almasi, P., de Menocal, P., et al. 1997. A pervasive millennial-scale cycle in North Atlantic Holocene and Glacial Climates. Science, **278**: 1257–1266. doi:10.1126/science.278.5341.1257.

Bond, G., Kromer, B., Beer, J., Muscheler, R., Evans, M.N., Showers, W., et al. 2001. Persistent solar influence on North

Atlantic climate during the Holocene. Science, **294**: 2130–2136. doi:10.1126/science.1065680.

Calvo, E., Grimalt, J., and Jansen, E. 2002. High resolution U_{37}^K sea surface temperature reconstruction in the Norwegian Sea during the Holocene. Quaternary Science Reviews, **21**: 1385–1394. doi:10.1016/S0277-3791(01)00096-8.

Comiso, J.C. 2002. A rapidly declining Arctic perennial ice cover. Geophysical Research Letters, **29**: No. 1956. doi:10.1029/2002GL015650.

Comiso, J.C. 2006. Abrupt decline in the Arctic winger sea ice cover. Geophysical Research Letters, **33**: No. L18504. doi:10.1029/2006GL027341.

Comiso, J.C., and Parkinson, C.L. 2004. Satellite-observed changes in the Arctic. Physics Today, **57**: 38–44. doi:10.1063/1.1801866.

Comiso, J.C., Parkinson, C.L., Gersten, R., and Stock, L. 2008. Accelerated decline in the Arctic sea ice cover. Geophysical Research Letters, **35**: No. L01703. doi:10.1029/2007GL031972.

Darby, D.A., and Bischof, J.F. 2004. A Holocene record of changing Arctic Ocean ice drift analogous to the effects of the Arctic Oscillation. Paleoceanography, **19**: No. PA1027. doi:10.1029/2003PA000961.

Darby, D.A., Bischof, J., Cutter, G., de Vernal, A., Hillaire-Marcel, C., Dwyer, G., et al. 2001. New record shows pronounced changes in Arctic Ocean circulation and climate. Eos, Transactions, American Geophysical Union, **82**: 601. doi:10.1029/01EO00345.

Darby, D.A., Jakobsson, M., and Polyak, L. 2005. Icebreaker expedition collects key Arctic seafloor and ice data. Eos, Transactions, American Geophysical Union, **86**: 549–556. doi:10.1029/2005EO520001.

de Vernal, A., and Hillaire-Marcel, C. 2000. Sea-ice, sea-surface salinity and the halo/thermocline structure in the northern North Atlantic: modern versus full glacial conditions. Quaternary Science Reviews, **19**: 65–85. doi:10.1016/S0277-3791(99)00055-4.

de Vernal, A., and Marret, F. 2007. Organic-walled dinoflagellates: tracers of sea-surface conditions, *In* Proxies in late Cenozoic paleoceanography. *Edited by* C. Hillaire-Marcel and A. de Vernal. Elsevier, Amsterdam, the Netherlands, pp. 371–408.

de Vernal, A., Larouche, A., and Richard, P.J.H. 1987. Evaluation of palynomorphs concentrations: do the aliquot and the marker-grain methods yield comparable results? Pollen and Spores, **29**: 291–304.

de Vernal, A., Turon, J.-L., and Guiot, J. 1994. Dinoflagellate cyst distribution in high latitude environments and quantitative reconstruction of sea-surface temperature, salinity and seasonality. Canadian Journal of Earth Sciences, **31**: 48–62. doi:10.1139/e94-006.

de Vernal, A., Henry, M., and Bilodeau, G. 1996. Techniques de préparation et d'analyse en micropaléontologie, Les cahiers du GEOTOP, **3**: 16–27.

de Vernal, A., Henry, M., Matthiessen, J., Mudie, P.J., Rochon, A., Boessenkool, K.P., et al. 2001. Dinoflagellates cyst assemblages as tracers of sea-surface conditions in the northern North Atlantic, Arctic and sub-Arctic seas: the new 'n = 677' database and its application for quantitative paleoceanographic reconstruction. Journal of Quaternary Science, **16**: 681–698. doi:10.1002/jqs.659.

de Vernal, A., Hillaire-Marcel, C., and Darby, D. 2005*a*. Variability of sea ice cover in the Chukchi Sea (western Arctic Ocean) during the Holocene. Paleoceanography, **20**: No. PA4018. doi:10.1029/2005PA001157.

de Vernal, A., Eynaud, F., Henry, M., Hillaire-Marcel, C., Londeix, L., Mangin, S., et al. 2005*b*. Reconstruction of sea-surface conditions at middle to high latitudes of the Northern Hemisphere during the Last Glacial Maximum (LGM) based on dinoflagellate cyst assemblages. Quaternary Science Reviews, **24**: 897–924. doi:10.1016/j.quascirev.2004.06.014.

de Vernal, A., Hillaire-Marcel, C., Solignac, S., Radi, T., and Rochon, A. 2008. reconstructing sea-ice conditions in the Arctic and subarctic prior to human observations. *In* Arctic Sea ice decline: observations, projections, mechanisms, and implications. *Edited by* E. Weaver. AGU Monograph, in press.

Dickson, R.R., Osborn, T.J., Hurrell, J.W., Meincke, J., Blindheim, J., Adlandsvik, B., et al. 2000. The Arctic Ocean response to the North Atlantic Oscillation. Journal of Climate, **13**: 2671–2696. doi:10.1175/1520-0442(2000)013<2671:TAORTT>2.0.CO;2.

Duplessy, J.-C., Ivanova, E., Murdmaa, I., Paterne, M., and Labeyrie, L. 2001. Holocene paleoceanography of the northern Barents Sea and variations of the northward heat transport by the Atlantic Ocean. Boreas, **30**: 2–16.

Duplessy, J.C., Cortijo, E., Ivanova, E., Khusid, T., Labeyrie, L., Levitan, M., Murdmaa, I., and Paterne, M. 2005. Paleoceanography of the Barents Sea during the Holocene. Paleoceanography, **20**: No. PA4004. doi:10.1029/2004PA001116.

Dyke, A.S., and Savelle, J.M. 2000. Holocene driftwood incursion to southwestern Victoria Island, Canadian Arctic Archipelago, and its significance to paleoceanography and archaeology. Quaternary Research, **54**: 113–120. doi:10.1006/qres.2000.2141.

Dyke, A.S., Hooper, J., and Savelle, J.M. 1996. A history of sea ice in the Canadian Arctic Archipelago based on postglacial remains of the Bowhead Whale (Balaena mysticetus). Arctic, **49**: 235–255.

Dyke, A.S., England, J., Reimnitz, E., and Jette, H. 1997. Changes in driftwood delivery to the Canadian Arctic Archipelago: The hypothesis of postglacial oscillations of the Transpolar Drift. Arctic, **50**: 1–16.

Forman, S.L., and Polyak, L. 1997. Radiocarbon content of prebomb marine mollusks and variations in the 14C reservoir age for coastal areas of the Barents and Kara seas, Russia. Geophysical Research Letters, **24**: 885–888. doi:10.1029/97GL00761.

Grootes, P.M., and Stuiver, M. 1997. Oxygen 18/16 variability in Greenland snow and ice with 10^{-3}- to 10^5-year time resolution. Journal of Geophysical Research, **102**: 26 455 – 26 470. doi:10.1029/97JC00880.

Grotefendt, K., Logemann, K., Quadfasel, D., and Ronski, S. 1998. Is the Arctic Ocean warming? Journal of Geophysical Research, **103**: 27 679 – 27 687. doi:10.1029/98JC02097.

Guiot, J., and de Vernal, A. 2007. Transfer functions: methods for quantitative paleoceanography based on microfossils. *In* Proxies in Late Cenozoic paleoceanography. *Edited by* C. Hillaire-Marcel and A. de Vernal. Elsevier, Amsterdam, the Netherlands, pp. 523–563.

Guiot, J., and Goeury, C. 1996. PPPbase, a software for statistical analysis of paleoecological data. Dendrochronologia, **14**: 295–300.

Head, M.J. 1996. Modern dinoflagellate cysts and their biological affinities. *In* Palynology: principles and applications. Vol. 3. *Edited by* J. Jansonius and D.C. McGregor. American Association of Stratigraphic Palynologists Foundation, pp. 1197–1248.

Hillaire-Marcel, C., de Vernal, A., Polyak, L., and Darby, D. 2004. Size-dependent isotopic composition of planktic foraminifers from Chukchi Sea vs. NW Atlantic sediments — implications for the Holocene paleoceanography of the western Arctic. Quaternary Science Reviews, **23**: 245–260. doi:10.1016/j.quascirev.2003.08.006.

IPCC. 2007. Climate Change 2007: The Physical Science Basis. *In* 4th assessment report of the Intergovernmental Panel on Climate

Change. *Edited by* S. Solomon, D. Qin, M. Manning, Z. Chen, M. Marquis, K.B. Averyt, M. Tignor, and H.L. Miller. Cambridge University Press, Cambridge, UK, and New York, 996 p.

Jordan, J.W. 2001. Late Quaternary sea level change in Southern Beringia: postglacial emergence of the Western Alaska Peninsula. Quaternary Science Reviews, **20**: 509–523. doi:10.1016/S0277-3791(00)00101-3.

Jordan, J.W., and Mason, O.K. 1999. 5000 year record of intertidal peat stratigraphy and sea level change from northwest Alaska. Quaternary International, **60**: 37–47. doi:10.1016/S1040-6182(99)00005-1.

Kang, H.-S., Won, E.-J., Shin, K.-H., and Yoon, H.I. 2007. Organic carbon and nitrogen composition in the sediment of the Kara Sea, Arctic Ocean during the Last Glacial Maximum to Holocene times. Geophysical Research Letters, **34**: No. L12607. doi:10.1029/2007GL030068.

Keeling, C.D., and Whorf, T.P. 1997. Possible forcing of global temperature by the oceanic tides. Proceedings of the National Academy of Sciences, **94**: 8321–8328. doi:10.1073/pnas.94.16.8321.

Keigwin, L.D., Donnelly, J.P., Cook, M.S., Driscoll, N.W., and Brigham-Grette, J. 2006. Rapid sea-level rise and Holocene climate in the Chukchi Sea. Geology, **34**: 861–864. doi:10.1130/G22712.1.

Klitgaard-Kristensen, D., Sejrup, H.P., and Haflidason, H. 2001. The last 18 ka fluctuations in Norwegian Sea surface conditions and implications for the magnitude of climatic change: Evidence from the North Sea. Paleoceanography, **16**: 455–467. doi:10.1029/1999PA000495.

Kunz-Pirrung, M. 2001. Dinoflagellate cyst assemblages in surface sediments of the Laptev Sea region (Arctic Ocean) and their relationship to hydrographic conditions. Journal of Quaternary Science, **16**: 637–649. doi:10.1002/jqs.647.

Kwok, R. 2000. Recent changes in Arctic Ocean sea ice motion associated with the North Atlantic Oscillation. Geophysical Research Letters, **27**: 775–778. doi:10.1029/1999GL002382.

Ledu, D., Rochon, A., de Vernal, A., and St-Onge, G. 2008. Palynological evidence of Holocene climate change in the eastern Arctic: a possible shift in the Arctic Oscillation at millennial time scale. Canadian Journal of Earth Sciences, **45**: this issue.

Levac, E., de Vernal, A., and Blake, W., Jr. 2001. Sea-surface conditions in northernmost Baffin Bay during the Holocene: palynological evidence. Journal of Quaternary Science, **16**: 353–363. doi:10.1002/jqs.614.

Mason, O.K., and Jordan, J.W. 2002. Minimal late Holocene sea level rise in the Chukchi Sea: arctic insensitive to global change. Global and Planetary Change, **32**: 13–23. doi:10.1016/S0921-8181(01)00146-1.

Matthews, J. 1969. The assessment of a method for the determination of absolute pollen frequencies. The New Phytologist, **68**: 161–166. doi:10.1111/j.1469-8137.1969.tb06429.x.

Matthiessen, J., de Vernal, A., Head, M., Okolodkov, Y., Zonneveld, K., and Harland, R. 2005. Modern organic-walled dinoflagellate cysts in Arctic marine environments and their (paleo-) environmental significance. Palaeontologische Zeitschrift, **79**: 3–51.

Mayewski, P.A., Rohling, E.E., Stager, J.C., Karlen, W., Maasch, K.A., Meeker, L.D., et al. 2004. Holocene climate variability. Quaternary Research, **62**: 243–255. doi:10.1016/j.yqres.2004.07.001.

McLaughlin, F.A., Carmack, E.C., Macdonald, R.W., and Bishop, J.K.B. 1996. Physical and geochemical properties across the Atlantic/Pacific water mass front in the southern Canadian Basin. Journal of Geophysical Research, **101**: 1183–1197. doi:10.1029/95JC02634.

McNeely, R., Dyke, A.S., and Southon, J.R. 2006. Canadian marine reservoir ages, preliminary data assessment. Geological Survey of Canada, Open File 5049.

Meier, W., Stroeve, J., Fetterer, F., and Knowles, K. 2005. Reductions in Arctic sea ice cover no longer limited to summer. Eos, Transactions of the American Geophysical Union, **86**: 326–327. doi:10.1029/2005EO360003.

Morison, J., Steele, M., and Andersen, R. 1998. Hydrography of the upper Arctic Ocean measured from the nuclear submarine U.S.S. Pargo. Deep-Sea Research Part I Oceanographic Research Papers, **45**: 15–38. doi:10.1016/S0967-0637(97)00025-3.

Mudie, P.J., and Rochon, A. 2001. Distribution of dinoflagellates cysts in the Canadian Arctic marine region. Journal of Quaternary Science, **16**: 603–620. doi:10.1002/jqs.658.

Mudie, P.J., Harland, R., Matthiessen, J., and de Vernal, A. 2001. Marine dinoflagellate cysts and high latitude Quaternary paleoenvironmental reconstructions: an introduction. Journal of Quaternary Science, **16**: 595–602. doi:10.1002/jqs.660.

Mudie, P.J., Rochon, A., Prins, M.A., Soenarjo, D., Troelstra, S.R., Levac, E., et al. 2006. Late Pleistocene–Holocene marine geology of Nares Strait region: Paleoceanography from foraminifera and dinoflagellate cysts, sedimentology and stable isotopes. Polarforschung, **74**: 1–3.

Mueller-Lupp, T., Bauch, H.A., Erlenkeuser, H., Hefter, J., Kassens, H., and Thiede, J. 2000. Changes in the deposition of terrestrial organic matter on the Laptev Sea shelf during the Holocene: evidence from stable carbon isotopes. International Journal of Earth Sciences, **89**: 563–568. doi:10.1007/s005310000128.

O'Brien, S.R., Mayewski, P.A., Meeker, L.D., Meese, D.A., Twickler, M.S., and Whitlow, S.I. 1995. Complexity of Holocene climate as reconstructed from a Greenland ice core. Science, **270**: 1962–1964. doi:10.1126/science.270.5244.1962.

Overland, J.E., and Wang, M. 2005. The Arctic climate paradox: the recent decrease of the Arctic Oscillation. Geophysical Research Letters, **32**: No. L06701. doi:10.1029/2004GL021752.

Parkinson, C.L., Cavalieri, D.J., Gloersen, P., Zwally, H.J., and Comiso, J.C. 1999. Arctic sea ice extents, areas, and trends, 1978–1996. Journal of Geophysical Research, **104**: 20 837 – 20 856. doi:10.1029/1999JC900082.

Paul, A., and Schulz, M. 2002. Holocene climate variability on centennial-to-millennial time scales: 2. Internal and forced oscillations as possible causes. *In* Climate development and history of the North Atlantic realm. *Edited by* G. Wefer, et al. Springer Verlag, Berlin and Heidelberg, Germany, pp. 55–73.

Polyak, L., and Mikhailov, V. 1996. Post-glacial environments of the southeastern Barents Sea: foraminiferal evidence. *In* Late Quaternary palaeoceanography of the North Atlantic margins. *Edited by* J.T. Andrews, W.E.N. Austin, H. Bergsten, and A.E. Jennings. Geological Society, London, UK.

Radi, T., and de Vernal, A. 2008. Dinocysts as proxy of primary productivity in mid-high latitudes of the Northern Hemisphere. Marine Micropaleontology, **68**: 84–114.

Radi, T., de Vernal, A., and Peyron, O. 2001. Relationship between dinoflagellates cyst assemblages in surface sediment and hydrographic conditions in the Bering and Chukchi seas. Journal of Quaternary Science, **16**: 667–680. doi:10.1002/jqs.652.

Rigor, I.G., and Wallace, J.M. 2004. Variations in the age of Arctic sea-ice and summer sea ice extent. Geophysical Research Letters, **31**: No. L09401. doi:10.1029/2004GL019492.

Rochon, A., Scott, D.B., Schell, T.M., Blasco, S., Bennett, R.J., and Mudie, P.J. 2006. Evolution of sea Surface Conditions During the Holocene: Comparison Between Eastern (Baffin Bay and Hudson Strait) and Western (Beaufort Sea) Canadian Arctic.

American Geophysical Union, Fall Meeting 2006, abstract #U43B-0867.

Sarnthein, M., van Kreveld, S., Erlenkeuser, H., Grootes, P.M., Kucera, M., Pflaumann, U., and Schulz, M. 2003. Centennial-to-millennial-scale periodicities of Holocene climate and sediment injections off the western Barents shelf, 75°N. Boreas, **32**: 447–461. doi:10.1080/03009480301813.

Schulz, M., and Paul, A. 2002. Holocene climate variability on centennial-to-millennial time scales: 1. Climate records from the North-Atlantic realm. *In* Climate development and history of the North Atlantic realm. *Edited by* G. Wefer et al. Springer-Verlag, Berlin and Heidelberg, Germany, pp. 41–54.

Serreze, M.C., Walsh, J.E., Chapin, F.S. III, Osterkamp, T., Dyurgerov, M., Romanovsky, V., et al. 2000. Observational evidence of recent change in the northern high-latitude environment. Climatic Change, **46**: 159–207. doi:10.1023/A:1005504031923.

Serreze, M.C., Maslanik, J.A., Scambos, T.A., Fetterer, F., Stroeve, J., Knowles, K., et al. 2003. A record minimum arctic sea ice extent and area in 2002. Geophysical Research Letters, **30**: No. 1110. doi:10.1029/2002GL016406.

Slubowska, M.A., Koc, N., Rasmussen, T.L., and Klitgaard-Kristensen, D. 2005. Changes in the flow of Atlantic water into the Arctic Ocean since the last deglaciation: Evidence from the northern Svalbard continental margin, 80°N. Paleoceanography, **20**: No. PA4014. doi:10.1029/2005PA001141.

Steele, M., and Boyd, T. 1998. Retreat of the cold halocline layer in the Arctic Ocean. Journal of Geophysical Research, **103**: 10 419 – 10 435. doi:10.1029/98JC00580.

Steele, M., Morison, J., Ermold, W., Rigor, I., and Ortmeyer, M. 2004. Circulation of summer Pacific halocline water in the Arctic Ocean. Journal of Geophysical Research, **109**: 1001029/2003JC002009.

Stroeve, J., Serreze, M., Drobot, S., Gearheard, S., Holland, M., Maslanik, J., Meier, W., and Scambos, T. 2008. Arctic sea ice extent plummets in 2007. Eos, Transactions, American Geophysical Union, **89**: 13–20. doi:10.1029/2008EO020001.

Stuiver, M., Reimer, P.J., and Reimer, R.W. 2005. CALIB 5.0. Available from http://calib.qub.ac.uk/calib/calib.html [accessed November 2006].

Thompson, D.W., and Wallace, J.M. 1998. The Arctic oscillation signature in the wintertime geopotential height and temperature fields. Geophysical Research Letters, **25**: 1297–1300. doi:10.1029/98GL00950.

Voronina, E., Polyak, L., de Vernal, A., and Peyron, O. 2001. Holocene variations of sea surface conditions in the southeastern Barents Sea, reconstructed from dinoflagellate cyst assemblages. Journal of Quaternary Science, **16**: 717–726. doi:10.1002/jqs.650.

Walsh, J.E., Chapman, W.L., and Shy, T.L. 1996. Recent decrease of sea level pressure in the Central Arctic. Journal of Climate, **9**: 480–486. doi:10.1175/1520-0442(1996)009<0480:RDOSLP>2.0.CO;2.

Yndestad, H. 2006. The influence of the lunar nodal cycle on Arctic climate. ICES Journal of Marine Science, **63**: 401–420. doi:10.1016/j.icesjms.2005.07.015.

Appendix A

Tables A1 and A2 appear on the following pages.

Table A1. Geochemical data for trigger core (Tc) and piston core (Pc) from site HLY0501-05.

Core	Section	Uncorrected depth (cm)	Age (years BP)	N_{tot} (wt.%)	C_{tot} (wt.%)	$CaCO_3$ (wt.%)	C_{org} (wt.%)	C_{org}/N	$\delta^{13}C$ (‰, PDB)
Tc	1	7–9.0	43.8	0.23	1.77	0.74	1.68	7.3	–22.52
Tc	1	11–13.0	68.8	0.24	1.71	0.73	1.63	6.9	na
Tc	1	19–21	118.8	0.21	1.58	0.62	1.50	7.2	na
Tc	1	27–29	168.8	0.20	1.56	0.45	1.51	7.5	na
Tc	1	35–37	218.8	0.21	1.54	0.61	1.47	6.9	–22.35
Tc	1	43–45	268.8	0.21	1.56	0.54	1.50	7.0	na
Tc	1	51–53	318.8	0.21	1.60	0.59	1.53	7.4	na
Tc	1	59–61	368.8	0.21	1.49	0.56	1.42	6.9	na
Tc	1	67–69	418.8	0.20	1.48	0.56	1.42	7.1	–22.46
Tc	1	75–77	468.8	0.20	1.55	0.68	1.47	7.3	na
Tc	1	83–85	518.8	0.20	1.51	0.47	1.45	7.1	na
Tc	1	91–93	568.8	0.20	1.57	0.76	1.48	7.4	na
Tc	1	99–101	618.8	0.21	1.61	0.57	1.54	7.5	–22.73
Pc	1	12–14.0	1296.1	0.20	1.56	0.44	1.51	7.7	–22.74
Pc	1	20–22	1353.4	0.19	1.61	0.63	1.53	8.2	na
Pc	1	28–30	1410.7	0.20	1.54	0.59	1.47	7.4	na
Pc	1	36–38	1468.0	0.20	1.56	0.57	1.49	7.6	na
Pc	1	44–46	1525.3	0.20	1.59	0.64	1.51	7.5	–22.84
Pc	1	52–54	1582.6	0.20	1.57	0.48	1.51	7.5	na
Pc	1	60–62	1639.9	0.20	1.58	0.71	1.49	7.6	na
Pc	1	68–70	1697.2	0.20	1.54	0.69	1.46	7.4	na
Pc	1	76–78	1754.4	0.20	1.56	0.48	1.50	7.6	–22.96
Pc	1	84–86	1811.7	0.20	1.56	0.72	1.48	7.6	na
Pc	1	92–94	1869.0	0.19	1.56	0.64	1.48	7.8	na
Pc	1	100–102	1926.3	0.21	1.58	0.60	1.51	7.2	na
Pc	2	109.5–111.5	1994.3	0.19	1.57	0.70	1.49	7.8	–23.07
Pc	2	117.5–119.5	2051.6	0.19	1.55	0.55	1.48	7.8	na
Pc	2	125.5–127.5	2108.9	0.19	1.55	0.64	1.47	7.8	na
Pc	2	133.5–135.5	2166.2	0.19	1.59	0.53	1.53	8.0	na
Pc	2	141.5–143.5	2223.5	0.18	1.59	0.91	1.48	8.2	–23.18
Pc	2	149.5–151.5	2280.8	0.18	1.57	0.59	1.50	8.3	na
Pc	2	157.5–159.5	2338.1	0.17	1.44	0.64	1.36	8.0	na
Pc	2	165.5–167.5	2395.4	0.19	1.57	0.47	1.51	8.0	na
Pc	2	173.5–175.5	2452.6	0.18	1.57	0.49	1.51	8.4	–23.04
Pc	2	181.5–183.5	2509.9	0.17	1.52	0.50	1.46	8.6	na
Pc	2	189.5–191.5	2567.2	0.18	1.54	0.63	1.47	8.1	na
Pc	2	197.5–199.5	2624.5	0.18	1.52	0.73	1.43	8.0	na
Pc	2	205.5–207.5	2681.8	0.18	1.55	0.72	1.46	8.1	–22.97
Pc	2	213.5–215.5	2739.1	0.18	1.47	0.69	1.39	7.7	na
Pc	2	221.5–223.5	2796.4	0.18	1.59	0.71	1.51	8.2	na
Pc	2	229.5–231.5	2853.7	0.16	1.33	0.66	1.25	7.8	na
Pc	2	237.5–139.5	2911.0	0.18	1.56	0.81	1.46	8.1	–23.11
Pc	2	245.5–247.5	2968.2	0.18	1.53	0.84	1.43	7.9	na
Pc	2	253.5–255.5	3025.5	0.18	1.65	0.94	1.53	8.4	na
Pc	3	262–264	3086.4	0.19	1.59	0.84	1.49	7.9	na
Pc	3	270–272	3143.7	0.18	1.57	0.74	1.48	8.1	–23.12
Pc	3	278–280	3201.0	0.19	1.58	0.81	1.48	7.9	na
Pc	3	286–288	3258.3	0.18	1.57	0.86	1.47	8.0	na
Pc	3	294–296	3315.6	0.18	1.54	0.80	1.44	7.9	na
Pc	3	302–304	3372.8	0.18	1.52	0.71	1.43	8.0	–23.08
Pc	3	310–312	3430.1	0.18	1.55	0.73	1.46	8.0	na
Pc	3	318–320	3487.4	0.18	1.50	0.65	1.42	8.0	na
Pc	3	326–328	3544.7	0.18	1.49	0.58	1.42	8.0	na
Pc	3	334–336	3602.0	0.17	1.48	0.70	1.39	8.1	–23.24
Pc	3	342–344	3659.3	0.18	1.54	0.71	1.45	8.1	na
Pc	3	350–352	3716.6	0.18	1.53	0.71	1.44	8.0	na
Pc	3	358–360	3773.9	0.18	1.54	0.81	1.44	8.1	na
Pc	3	366–368	3831.2	0.18	1.53	0.77	1.44	8.0	–23.31
Pc	3	374–376	3888.4	0.17	1.52	0.77	1.42	8.2	na

Table A1 (*continued*).

Core	Section	Uncorrected depth (cm)	Age (years BP)	N_{tot} (wt.%)	C_{tot} (wt.%)	$CaCO_3$ (wt.%)	C_{org} (wt.%)	C_{org}/N	$\delta^{13}C$ (‰, PDB)
Pc	3	382–384	3945.7	0.17	1.52	0.73	1.43	8.3	na
Pc	3	390–392	4003.0	0.19	1.65	1.06	1.52	8.0	na
Pc	3	398–400	4060.3	0.18	1.61	0.86	1.51	8.2	–23.3
Pc	3	404–406	4103.3	0.18	1.56	0.80	1.46	8.3	na
Pc	4	411–413	4153.4	0.18	1.59	0.75	1.50	8.5	na
Pc	4	419–421	4210.7	0.18	1.58	0.88	1.48	8.2	na
Pc	4	427–429	4268.0	0.18	1.56	0.87	1.46	8.3	–23.42
Pc	4	435–437	4325.3	0.18	1.58	0.84	1.48	8.3	na
Pc	4	443–445	4382.6	0.17	1.57	0.65	1.49	8.6	na
Pc	4	451–453	4439.8	0.17	1.52	0.86	1.42	8.3	na
Pc	4	459–461	4497.1	0.17	1.56	0.96	1.44	8.3	–23.36
Pc	4	467–469	4554.4	0.17	1.53	0.81	1.43	8.3	na
Pc	4	475–477	4611.7	0.18	1.59	0.95	1.47	8.4	na
Pc	4	483–485	4669.0	0.17	1.56	0.93	1.45	8.4	na
Pc	4	491–493	4712.1	0.17	1.61	0.86	1.51	8.9	–23.42
Pc	4	499–501	4755.2	0.18	1.61	0.93	1.50	8.5	na
Pc	4	507–509	4798.3	0.17	1.57	0.90	1.47	8.5	na
Pc	4	515–517	4841.4	0.17	1.61	0.91	1.50	8.6	na
Pc	4	523–525	4884.4	0.18	1.60	0.86	1.50	8.4	–23.44
Pc	4	531–533	4927.5	0.17	1.59	1.01	1.46	8.5	na
Pc	4	539–541	4970.6	0.17	1.54	0.85	1.44	8.7	na
Pc	4	547–549	5013.7	0.17	1.58	1.08	1.45	8.7	na
Pc	4	553–554	5046.0	0.17	1.60	1.08	1.47	8.7	–23.6
Pc	5	560.5–562.5	5086.4	0.18	1.59	0.87	1.48	8.5	na
Pc	5	568.5–570.5	5129.5	0.18	1.58	1.10	1.45	8.1	na
Pc	5	576.5–578.5	5160.4	0.18	1.56	0.93	1.45	8.2	na
Pc	5	584.5–586.5	5191.2	0.18	1.58	0.95	1.46	8.2	–23.5
Pc	5	592.5–594.5	5222.1	0.17	1.57	1.02	1.45	8.4	na
Pc	5	600.5–602.5	5253.0	0.17	1.52	0.99	1.40	8.2	na
Pc	5	608.5–610.5	5283.8	0.17	1.56	1.03	1.43	8.3	na
Pc	5	616.5–618.5	5314.7	0.17	1.53	1.03	1.40	8.1	–23.56
Pc	5	624.5–626.5	5345.6	0.17	1.56	0.98	1.44	8.4	na
Pc	5	632.5–634.5	5376.4	0.17	1.56	0.93	1.45	8.4	na
Pc	5	640.5–642.5	5407.3	0.17	1.61	0.93	1.50	8.9	na
Pc	5	648.5–650.5	5438.2	0.18	1.61	0.90	1.50	8.6	–23.58
Pc	5	656.5–658.5	5469.0	0.17	1.57	1.04	1.45	8.4	na
Pc	5	664.5–666.5	5499.9	0.17	1.61	0.96	1.49	8.6	na
Pc	5	672.5–674.5	5530.8	0.18	1.60	0.91	1.49	8.4	na
Pc	5	680.5–682.5	5561.6	0.17	1.60	0.79	1.51	9.0	–23.66
Pc	5	688.5–690.5	5592.5	0.17	1.54	0.84	1.44	8.7	na
Pc	5	696.5–698.5	5644.1	0.17	1.58	0.86	1.48	8.8	na
Pc	5	704.5–706.5	5695.7	0.17	1.60	0.87	1.49	8.9	na
Pc	6	711–713	5737.7	0.16	1.53	0.83	1.43	9.0	–23.7
Pc	6	719–721	5789.3	0.17	1.55	0.93	1.44	8.7	na
Pc	6	727–729	5840.9	0.17	1.59	0.93	1.47	8.8	na
Pc	6	735–737	5892.5	0.16	1.59	1.08	1.46	9.0	na
Pc	6	743–745	5944.2	0.16	1.59	1.06	1.46	9.1	–23.8
Pc	6	751–752	5995.8	0.16	1.58	1.15	1.45	8.9	na
Pc	6	759–761	6047.4	0.16	1.55	1.10	1.41	8.8	na
Pc	6	767–769	6099.0	0.16	1.53	1.05	1.41	9.0	na
Pc	6	775–777	6150.6	0.16	1.57	1.02	1.45	8.8	–23.92
Pc	6	783–785	6202.3	0.17	1.57	0.92	1.46	8.7	na
Pc	6	791–793	6253.9	0.16	1.53	0.92	1.42	9.1	na
Pc	6	799–801	6305.5	0.16	1.57	0.85	1.47	9.2	na
Pc	6	807–809	6361.3	0.16	1.54	1.01	1.41	8.9	–23.97
Pc	6	815–817	6417.1	0.15	1.51	1.15	1.38	9.2	na
Pc	6	823–825	6472.9	0.15	1.53	1.12	1.39	9.1	na
Pc	6	831–833	6528.7	0.16	1.50	0.95	1.38	8.5	na
Pc	6	839–841	6584.5	0.16	1.49	1.02	1.37	8.5	–24.11

Table A1 (*continued*).

Core	Section	Uncorrected depth (cm)	Age (years BP)	N_{tot} (wt.%)	C_{tot} (wt.%)	$CaCO_3$ (wt.%)	C_{org} (wt.%)	C_{org}/N	$\delta^{13}C$ (‰, PDB)
Pc	6	847–849	6640.3	0.16	1.49	1.03	1.37	8.6	na
Pc	6	855–857	6696.1	0.16	1.54	0.91	1.43	9.1	na
Pc	7	863.5–865.5	6755.4	0.15	1.48	1.12	1.35	8.8	na
Pc	7	871.5–873.5	6811.2	0.15	1.46	1.12	1.32	8.8	–24.07
Pc	7	879.5–881.5	6867.0	0.15	1.48	1.07	1.35	9.0	na
Pc	7	887.5–889.5	6922.8	0.15	1.43	0.78	1.34	9.0	na
Pc	7	895.5–897.5	6978.6	0.15	1.50	1.26	1.35	8.8	na
Pc	7	903.5–905.5	7034.4	0.16	1.49	1.02	1.37	8.7	–24.14
Pc	7	911.5–913.5	7090.2	0.16	1.53	1.21	1.38	8.5	na
Pc	7	919.5–921.5	7146.0	0.15	1.50	1.21	1.35	8.8	na
Pc	7	927.5–929.5	7201.8	0.16	1.48	1.13	1.35	8.4	na
Pc	7	935.5–937.5	7257.6	0.15	1.39	1.40	1.22	7.9	–24.15
Pc	7	943.5–945.5	7313.4	0.16	1.45	1.05	1.32	8.3	na
Pc	7	951.5–953.5	7369.2	0.16	1.41	1.11	1.27	8.2	na
Pc	7	959.5–961.5	7425.0	0.16	1.47	1.32	1.31	8.2	na
Pc	7	967.5–969.5	7480.8	0.16	1.51	1.55	1.33	8.5	–24.25
Pc	7	975.5–977.5	7536.6	0.16	1.48	1.15	1.34	8.4	na
Pc	7	983.5–985.5	7592.4	0.16	1.47	1.18	1.32	8.5	na
Pc	7	991.5–993.5	7648.2	0.16	1.49	1.17	1.35	8.3	na
Pc	7	999.5–1001.5	7704.0	0.16	1.50	1.29	1.34	8.4	–24.39
Pc	7	1007.5–1009.5	7759.8	0.16	1.50	1.28	1.35	8.5	na
Pc	8	1016–1018	7819.1	0.16	1.51	1.34	1.35	8.7	na
Pc	8	1024–1026	7874.9	0.15	1.48	1.26	1.33	8.6	na
Pc	8	1032–1034	7930.7	0.16	1.53	1.42	1.36	8.8	–24.57
Pc	8	1040–1042	7986.5	0.15	1.50	1.32	1.35	8.9	na
Pc	8	1048–1050	8042.3	0.15	1.49	1.25	1.34	9.2	na
Pc	8	1056–1058	8098.1	0.14	1.45	1.19	1.30	9.4	na
Pc	8	1064–1066	8153.9	0.14	1.44	1.13	1.30	9.5	na
Pc	8	1072–1074	8209.7	0.15	1.50	1.10	1.36	9.4	na
Pc	8	1080–1082	8265.5	0.15	1.45	1.28	1.30	8.9	na
Pc	8	1088–1090	8321.3	0.13	1.27	1.29	1.12	8.8	na
Pc	8	1096–1098	8377.1	0.13	1.34	1.38	1.17	8.8	–24.74
Pc	8	1104–1106	8432.9	0.13	1.28	1.42	1.11	8.7	na
Pc	8	1112–1114	8488.7	0.12	1.20	1.46	1.03	8.6	na
Pc	8	1120–1122	8544.5	0.13	1.28	1.67	1.08	8.6	na
Pc	8	1128–1130	8600.3	0.12	1.27	1.68	1.07	8.6	–24.95
Pc	8	1136–1138	8656.1	0.12	1.22	1.51	1.04	8.4	na
Pc	8	1144–1146	8711.9	0.11	1.12	1.58	0.93	8.4	na
Pc	8	1152–1154	8767.7	0.12	1.17	1.52	0.98	8.5	na
Pc	8	1160–1162	8823.5	0.11	1.13	1.57	0.94	8.6	–24.95
Pc	9	1166.5–1168.5	8868.9	0.11	1.14	1.43	0.97	8.6	na
Pc	9	1174.5–1176.5	8924.7	0.11	1.14	1.45	0.96	8.5	–25
Pc	9	1182.5–1184.5	8980.5	0.11	1.10	1.41	0.93	8.7	na
Pc	9	1190.5–1192.5	9036.3	0.11	1.09	1.41	0.92	8.5	–24.94
Pc	9	1198.5–1200.5	9092.1	0.10	1.04	1.48	0.86	8.4	na
Pc	9	1206.5–1208.5	9147.9	0.10	1.02	1.59	0.83	8.3	–25.02
Pc	9	1214.5–1216.5	9203.7	0.11	1.01	1.43	0.84	8.0	na
Pc	9	1222.5–1224.5	9259.5	0.10	1.01	1.42	0.84	8.6	na
Pc	9	1230.5–1232.5	9315.3	0.10	1.03	1.48	0.85	8.7	na
Pc	9	1238.5–1240.5	9371.1	0.10	1.02	1.49	0.84	8.7	–25.09
Pc	9	1246.5–1248.5	unknown	0.10	1.01	na	na	na	na
Pc	9	1254.5–1256.5	unknown	0.11	1.25	na	na	na	–25.09
Pc	9	1262.5–1264.5	unknown	0.08	1.60	na	na	na	na
Pc	9	1270.5–1272.5	unknown	0.09	1.32	na	na	na	–25.15
Pc	9	1278.5–1280.5	unknown	0.08	1.40	na	na	na	na
Pc	9	1284.5–1286.5	unknown	0.08	1.60	na	na	na	–25.38
Pc	10	1289.5–1291.5	unknown	0.09	1.49	na	na	na	na
Pc	10	1297.5–1299.5	unknown	0.11	1.51	na	na	na	–26.06
Pc	10	1305.5–1307.5	unknown	0.12	1.40	na	na	na	na

Table A1 (*concluded*).

Core	Section	Uncorrected depth (cm)	Age (years BP)	N_{tot} (wt.%)	C_{tot} (wt.%)	$CaCO_3$ (wt.%)	C_{org} (wt.%)	C_{org}/N	$\delta^{13}C$ (‰, PDB)
Pc	10	1313.5–1315.5	unknown	0.11	1.74	na	na	na	–25.95
Pc	10	1321.5–1323.5	unknown	0.09	1.82	na	na	na	na
Pc	10	1329.5–1331.5	unknown	0.10	1.23	na	na	na	–24.99
Pc	10	1337.5–1339.5	unknown	0.09	1.39	na	na	na	na
Pc	10	1345.5–1347.5	unknown	0.10	1.49	na	na	na	–25.13
Pc	10	1353.5–1355.5	unknown	0.08	0.67	na	na	na	na
Pc	10	1361.5–1363.5	unknown	0.08	0.64	na	na	na	–24.69
Pc	10	1369.5–1371.5	unknown	0.08	0.61	na	na	na	na
Pc	10	1377.5–1379.5	unknown	0.10	1.24	na	na	na	–25.33
Pc	10	1385.5–1387.5	unknown	0.07	1.68	na	na	na	na
Pc	10	1393.5–1395.5	unknown	0.09	0.86	na	na	na	na
Pc	10	1401.5–1403.5	unknown	0.09	1.18	na	na	na	na
Pc	10	1409.5–1411.5	unknown	0.10	1.28	na	na	na	–25.88
Pc	10	1417.5–1419.5	unknown	0.10	1.24	na	na	na	na
Pc	10	1425.5–1427.5	unknown	0.09	1.14	na	na	na	–25.58
Pc	10	1433.5–1435.5	unknown	0.09	1.10	na	na	na	na
Pc	11	1447–1449	unknown	0.11	1.16	na	na	na	na
Pc	11	1455–1457	unknown	0.11	1.11	na	na	na	na
Pc	11	1463–1465	unknown	0.10	1.15	na	na	na	–25.87
Pc	11	1471–1473	unknown	0.10	1.17	na	na	na	na
Pc	11	1479–1481	unknown	0.10	1.23	na	na	na	–25.81
Pc	11	1487–1489	unknown	0.10	1.59	na	na	na	na
Pc	11	1495–1497	unknown	0.09	1.50	na	na	na	–25.71
Pc	11	1503–1505	unknown	0.10	1.45	na	na	na	na
Pc	11	1511–1513	unknown	0.10	1.55	na	na	na	–26.19
Pc	11	1519–1521	unknown	0.09	1.43	na	na	na	na
Pc	11	1527–1529	unknown	0.09	1.47	na	na	na	–25.74
Pc	11	1535–1537	unknown	0.08	1.53	na	na	na	na
Pc	11	1543–1545	unknown	0.09	1.39	na	na	na	–25.86
Pc	11	1551–1553	unknown	0.11	1.05	na	na	na	na
Pc	11	1559–1661	unknown	0.10	0.98	na	na	na	na
Pc	11	1567–1569	unknown	0.09	0.82	na	na	na	na
Pc	11	1575–1577	unknown	0.10	0.95	na	na	na	na
Pc	11	1583–1585	unknown	0.11	0.95	na	na	na	na
Pc	12	1592–1594	unknown	0.10	1.08	na	na	na	na
Pc	12	1600–1602	unknown	0.10	0.86	na	na	na	na
Pc	12	1614–1616	unknown	0.10	0.86	na	na	na	na
Pc	12	1622–1624	unknown	0.09	0.83	na	na	na	na
Pc	12	1630–1632	unknown	0.09	0.84	na	na	na	na
Pc	12	1638–1640	unknown	0.10	0.99	na	na	na	na
Pc	12	1646–1648	unknown	0.10	1.02	na	na	na	na
Pc	12b	1654–1656	unknown	0.11	0.97	na	na	na	na
Pc	12b	1662–1664	unknown	0.11	0.99	na	na	na	na

Note: N_{tot}, total nitrogen; C_{tot}, total carbon; C_{org}, organic carbon; na, not available.

Table A2. Dinocyst taxa in core HLY0501-05.

Core	Section	Uncorrected depth (cm)	Age (years BP)	BTEP (%)	IACU (%)	IPAL (%)	IPAR (%)	IPAT (%)	ISPH (%)	ISTR (%)	ISPP (%)	NLAB (%)	OCEN (%)	PRET (%)
Tc	1	7–9.0	43.75	0	0	0	0	0	0	0	0	0	18.96	0
Tc	1	11–13.0	68.75	0	0	0	0	0	0	0	0	0	35.27	0
Tc	1	19–21	118.75	0	0	0	0	0	0	0	0	0	21.01	0
Tc	1	27–29	168.75	0	0	0	0	0	0	0	0	0	21.20	0
Tc	1	35–37	218.75	0	0	0	0	0	0	0	0	0	10.68	0
Tc	1	43–45	268.75	0	0	0	0	0	0	0	0	0	13.16	0
Tc	1	51–53	318.75	0	0	0.54	0	0	0	0	0	0	10.22	0
Tc	1	59–61	368.75	0	0	0	0	0	0	0	0	0	9.17	0
Tc	1	67–69	418.75	0	0	0	0	0	0	0	0	0	5.62	0
Tc	1	75–77	468.75	0	0	0	0	0	0	0	0	0	12.46	0
Tc	1	83–85	518.75	0	0	0	0	0	0	0	0	0	14.56	0
Tc	1	91–93	568.75	0	0	0	0	0	0	0	0	0	10.13	0
Tc	1	99–101	618.75	0	0	0	0	0	0	0	0	0.55	11.54	0
Pc	1	12–14.0	1296.1	0.24	0	0.48	0.24	0	0	0	0	0	16.18	0
Pc	1	20–22	1353.4	0.89	0	0.30	0	0	0	0	0	0.30	29.38	0
Pc	1	28–30	1410.7	0.60	0	0.30	0	0	0	0	0	0.30	26.81	0
Pc	1	36–38	1468	1.44	0	0.57	0	0	0	0	0	0.29	24.71	0
Pc	1	44–46	1525.3	0.28	0	0	0	0	0	0	0	0	23.73	0
Pc	1	52–54	1582.6	1.93	0	1.10	0	0	0	0	0	0	34.71	0
Pc	1	60–62	1639.9	0.52	0	0	0	0	0	0	0.26	0.26	30.91	0
Pc	1	68–70	1697.2	1.59	0.27	0	0	0	0	0	0	0.27	23.87	0
Pc	1	76–78	1754.4	0.53	0	0	0	0	0	0	0	0	27.66	0
Pc	1	84–86	1811.7	0.48	0	0	0	0	0	0	0	0	23.33	0
Pc	1	92–94	1869	0.21	0	0	0	0	0	0	0	0.21	8.58	0
Pc	1	100–102	1926.3	0.47	0	0	0	0	0	0	0	0	9.41	0
Pc	2	109.5–111.5	1994.3	0	0	0	0	0	0	0	0	0	15.89	0
Pc	2	117.5–119.5	2051.6	0	0	0	0	0	0	0	0	0	12.28	0
Pc	2	125.5–127.5	2108.9	0.24	0	0	0	0	0	0	0	0.24	14.88	0
Pc	2	133.5–135.5	2166.2	0	0	0	0	0	0	0	0	0	14.37	0
Pc	2	141.5–143.5	2223.5	0	0	0	0	0	0	0	0	0	14.26	0
Pc	2	149.5–151.5	2280.8	0	0	0	0	0	0	0	0	0	16.43	0
Pc	2	157.5–159.5	2338.1	0	0	0	0	0	0	0	0	0	27.78	0
Pc	2	165.5–167.5	2395.4	0	0	0	0	0	0	0	0	0	18.58	0
Pc	2	173.5–175.5	2452.6	0	0	0	0	0	0	0	0	0	15.03	0
Pc	2	181.5–183.5	2509.9	0	0	0.26	0	0	0	0	0	0	14.95	0
Pc	2	189.5–191.5	2567.2	0	0	0	0	0	0	0	0	0	13.70	0
Pc	2	197.5–199.5	2624.5	0	0	0	0	0	0	0	0	0	22.79	0
Pc	2	205.5–207.5	2681.8	0	0	0	0	0	0	0	0	0	12.98	0
Pc	2	213.5–215.5	2739.1	0	0	0.53	0	0	0	0	0	0	21.43	0
Pc	2	221.5–223.5	2796.4	0	0	0.53	0	0	0	0	0	0	20.79	0
Pc	2	229.5–231.5	2853.7	0	0	0	0	0	0	0	0	0	22.46	0
Pc	2	237.5–239.8	2911	0.48	0	0.24	0	0	0	0	0	0	18.18	0
Pc	2	245.5–247.5	2968.2	0	0	0.67	0	0	0	0	0	0	16.44	0
Pc	2	253.5–255.5	3025.5	0	0	0	0	0	0	0	0.30	0	21.13	0
Pc	3	262–264	3086.4	1.55	0	0	0	0	0	0	0	0	25.19	0
Pc	3	270–272	3143.7	0.29	0	0	0	0	0	0	0	0	24.64	0
Pc	3	278–280	3201	0	0	1.61	0	0	0	0	0	0	24.19	0
Pc	3	294–296	3315.6	0	0	2.14	0	0	0	0	0	0	29.95	0
Pc	3	302–304	3372.8	0	0	0	0	0	0	0	0	0	33.33	0
Pc	3	334–336	3602	0	0	0	0	0	0	0	0	0	24.24	0
Pc	3	366–368	3831.2	0.82	0	0	0	0	0	0	0	0	17.21	0
Pc	3	398–400	4060.3	0.0	0	0	0	0	0	0	0	0.50	24.12	0
Pc	4	427–429	4268	0.35	0	0	0	0	0	0	0	0	20.14	0
Pc	4	459–461	4497.1	0.0	0	0	0	0	0	0	0	0	15.02	0
Pc	4	475–477	4611.7	0.78	0	0	0	0	0	0	0	0	30.62	0
Pc	4	491–493	4712.1	1.21	0	0	0	0	0	0	0	0	20.97	0
Pc	4	523–525	4884.4	0	0	0.63	0	0	0	0	0.31	0	21.88	0
Pc	4	547–549	5013.7	0	0	0.50	0	0	0	0	0	0	21.59	0
Pc	5	568.5–570.5	5129.5	0	0	1.32	0	0	0	0	0	0	11.45	0
Pc	5	616.5–618.5	5314.7	0	0	0	0	0	0	0	0	0	28.92	0
Pc	5	640.5–642.5	5407.3	0	0	0.35	0	0	0	0	0	0	31.49	0
Pc	5	664.5–666.5	5499.9	0	0	0	0	0	0	0	0	0	32.31	0
Pc	5	688.5–690.5	5592.5	0	0	0.80	0	0	0	0	0	0	21.60	0
Pc	6	711–713	5737.7	0	0	0	0	0	0	0	0	0.73	30.66	0
Pc	6	735–737	5892.5	0	0	0	0	0	0	0	0	0	33.90	0
Pc	6	759–761	6047.4	0	0	0	0	0	0	0	0	0	32.58	0
Pc	6	815–817	6417.1	0	0	0	0	0	0	0	0	0	24.28	0
Pc	6	839–841	6584.5	0	0	1.30	0	0	0	0	0	0	38.96	0
Pc	7	863.5–865.5	6755.4	0	0	0	0	0	0	0	0	0	27.43	0
Pc	7	887.5–889.5	6922.8	0.40	0	0	0	0	0.40	0	0	0	29.25	0

SELO (%)	SRAM (%)	SFRI (%)	SSPP (%)	PDAL (%)	IMIN (%)	IMIC (%)	BSPP (%)	SNEP (%)	SQUA (%)	TAPP (%)	TVAR (%)	PSCH (%)	PARC (%)	PKOF (%)	PQUA (%)
2.45	0	0	0	51.38	8.26	1.83	17.13	0	0	0	0	0	0	0	0
0	0	0	0	33.82	15.27	2.18	13.09	0	0	0	0	0	0.36	0	0
0.84	0	0	0	34.45	26.47	5.88	11.34	0	0	0	0	0	0	0	0
2.12	0.71	0	0	19.08	14.84	4.24	37.81	0	0	0	0	0	0	0	0
1.64		0	0.27	52.6	5.48	3.01	26.30	0	0	0	0	0	0	0	0
3.51	0.88	0	0.29	42.98	2.92	2.63	33.63	0	0	0	0	0	0	0	0
2.15	0.27	0	0.27	46.24	10.48	2.15	27.69	0	0	0	0	0	0	0	0
0.92	0	0	0	50.15	4.59	2.45	32.72	0	0	0	0	0	0	0	0
0	0	0	0	54.14	5.62	2.96	31.66	0	0	0	0	0	0	0	0
0.30	0.30	0	0	68.25	6.82	1.48	10.39	0	0	0	0	0	0	0	0
1.15	0.38	0	0	55.17	10.73	2.30	15.71	0	0	0	0	0	0	0	0
0.27	1.33	0	0.53	63.2	10.4	3.47	10.67	0	0	0	0	0	0	0	0
1.65	0	0	0.55	12.09	39.56	0.55	33.52	0	0	0	0	0	0	0	0
0.97	0.72	0	0	39.13	9.90	0.72	30.68	0.48	0.24	0	0	0	0	0	0
1.19	0	0	0	26.71	3.26	0	36.80	0	1.19	0	0	0	0	0	0
0.60	0	0	0.30	23.80	2.71	0	43.67	0.90	0	0	0	0	0	0	0
1.15	0.29	0	0.57	15.52	2.87	0.57	51.44	0.00	0.57	0	0	0	0	0	0
1.69	0.85	0	0.28	34.46	1.41	0	36.44	0.00	0.85	0	0	0	0	0	0
1.10	1.65	0	0.28	19.56	1.10	0.83	36.64	0.28	0.83	0	0	0	0	0	0
1.04	0.52	0	0	26.23	1.82	1.04	37.14	0	0.26	0	0	0	0	0	0
2.92	1.06	0	0.27	23.87	3.98	1.06	40.85	0	0	0	0	0	0	0	0
2.66	0.27	0	0.27	32.18	2.13	0.80	32.98	0	0.53	0	0	0	0	0	0
2.86	0.71	0	0.24	36.90	1.67	0.71	32.14	0	0.95	0	0	0	0	0	0
0.21	0.21	0	0	44.42	4.08	1.93	39.48	0	0.64	0	0	0	0	0	0
1.41	0.24	0	0.24	55.76	2.59	1.65	27.76	0	0.47	0	0	0	0	0	0
2.12	0	0	0.21	38.77	4.03	1.91	36.44	0	0.64	0	0	0	0	0	0
0.44	0.66	0	0.44	39.47	3.29	4.17	38.38	0	0.88	0	0	0	0	0	0
0.98	0.49	0	0	38.78	2.44	3.66	37.80	0	0.49	0	0	0	0	0	0
0.60	0.80	0	0.40	35.53	3.39	3.59	40.92	0.20	0.20	0	0	0	0	0	0
1.06	0.43	0	0.64	42.77	2.77	2.55	35.53	0	0	0	0	0	0	0	0
1.41	0	0	0.94	36.62	2.58	1.64	40.14	0	0.23	0	0	0	0	0	0
2.92	0.29	0	0	35.96	1.46	0.29	30.99	0	0.29	0	0	0	0	0	0
1.37	0.27	0	0	54.92	0.82	0.82	22.95	0	0.27	0	0	0	0	0	0
3.37	0.52	0	0.26	41.71	1.55	0.78	36.79	0	0	0	0	0	0	0	0
2.06	0.52	0	0	54.90	1.03	1.29	25.00	0	0	0	0	0	0	0	0
1.29	0	0	0	56.07	3.10	2.84	22.74	0	0.26	0	0	0	0	0	0
2.45	0.49	0	0	44.12	1.23	1.47	27.45	0	0	0	0	0	0	0	0
1.92	0.24	0	0.24	50.72	5.77	2.88	25.24	0	0	0	0	0	0	0	0
1.59	0	0	0	39.95	5.56	2.38	28.31	0	0.26	0	0	0	0	0	0
2.89	0.79	0	0.26	38.16	5.26	5.00	26.32	0	0	0	0	0	0	0	0
0.97	0.24	0	0.24	42.51	6.04	1.69	25.36	0	0.48	0	0	0	0	0	0
1.67	0.48	0	0.24	53.59	1.20	1.44	22.49	0	0.00	0	0	0	0	0	0
0.67	0	0	0	55.37	2.01	0.34	24.16	0	0.34	0	0	0	0	0	0
0	0.30	0	0.60	33.93	1.79	0.89	40.48	0	0.60	0	0	0	0	0	0
1.94	0	0	0	29.07	6.98	0	35.27	0	0	0	0	0	0	0	0
2.90	0	0	0.29	24.64	1.74	2.61	42.32	0.29	0.29	0	0	0	0	0	0
2.42	0	0	0	31.45	5.65	0	29.84	1.61	0	0	0	0	0	0	3.23
2.67	0.53	0	0	47.59	1.60	0	12.83	1.60	0	0	0	0	0	0	1.07
3.51	0	0	0	24.56	3.51	1.75	33.33	0	0	0	0	0	0	0	0
0.51	0	0	1.01	52.53	9.60	0	12.12	0	0	0	0	0	0	0	0
0.82	0	0	1.23	32.38	24.59	0.41	21.31	0	0.82	0	0	0	0	0.41	0
0.50	0	0	0	52.26	9.55	1.01	10.05	0	1.51	0	0	0	0	0	0.50
0.71	0	0	0	55.12	14.84	0.71	7.77	0	0	0	0	0	0	0.35	0
1.47	0	0	0.37	64.47	10.62	0.37	6.59	0	0.37	0	0	0	0	0	0.73
2.71	0	0	0.39	39.53	5.81	0	19.77	0	0.39	0	0	0	0	0	0
2.02	0.81	0	0.40	57.26	6.05	0.40	10.08	0	0.40	0	0	0	0	0.40	0
1.56	0.31	0	0	52.81	5.63	0	15.94	0	0.94	0	0	0	0	0	0
2.98	0.74	0	0	42.93	8.44	0	21.84	0	0.74	0	0	0.25	0	0	0
2.64	0	0	0	36.12	11.89	0	35.68	0	0.88	0	0	0	0	0	0
6.43	0.40	0	0	33.73	9.64	0	19.68	0	1.20	0	0	0	0	0	0
3.11	0	0	0	26.99	11.42	0.35	25.61	0	0.69	0	0	0	0	0	0
0	0	1.02	0.34	11.22	20.07	0	32.31	0	1.70	0	0	0	0.68	0	0.34
0	0	0	0.80	19.20	20.80	2.40	33.60	0	0	0	0	0	0.80	0	0
0	0	2.19	0	6.57	16.79	1.46	41.61	0	0	0	0	0	0	0	0
0	0	2.26	1.69	14.12	27.68	0	18.64	0	0.56	0	0	0	0	0	1.13
0	0	0.76	0	8.33	37.12	1.52	18.18	0	0.76	0	0	0	0	0	0.76
1.73	0.58	0	1.16	35.26	15.03	1.16	19.08	0	0.58	0	0	0	0	0	1.16
2.60	0	0	0	22.08	32.47	0	0	0	1.30	0	0	0	1.30	0	0
0.88	0.88	0	0	18.58	26.55	2.65	21.24	0	0.88	0	0	0	0	0	0.88
2.37	0.40	0	0.40	11.46	22.92	4.35	27.27	0	0.79	0	0	0	0	0	0

Table A2 (*concluded*).

Core	Section	Uncorrected depth (cm)	Age (years BP)	BTEP (%)	IACU (%)	IPAL (%)	IPAR (%)	IPAT (%)	ISPH (%)	ISTR (%)	ISPP (%)	NLAB (%)	OCEN (%)	PRET (%)
Pc	7	911.5–913.5	7090.2	0	0	0	0	0	0	0	0	0.72	33.09	0
Pc	7	935.5–937.5	7257.6	0	0	0.68	0	0	0	0	0	0	21.23	0
Pc	7	959.5–961.5	7425	0	0	0	0	0	0	0	0	0	15.79	0
Pc	7	983.5–985.5	7592.4	0	0	0	0	0	0	0	0	0	23.58	0
Pc	8	1032–1034	7930.7	0	0	0	0	0	0	0	0	0	26.39	0.69
Pc	8	1056–1058	8098.1	0	0	0	0	0	0	0	0	0	22.15	0
Pc	8	1080–1082	8265.5	0	0	0.85	0	0	0	0	0	0	16.24	0
Pc	8	1128–1130	8600.3	0	0	1.30	0	0	0	0	0	0	23.38	0
Pc	8	1152–1154	8767.7	0	0	1.77	0	0	0	0	0	0	54.42	0
Pc	9	1174.5–1176.5	8980.5	0	0	0	0	0	0	0	0	0	45.51	0
Pc	9	1198.5–1200.5	9092.1	0.32	0	0	0	0	0	0.32	0	0.32	61.36	0
Pc	9	1222.5–1224.5	9259.5	0	0	0	0	0	0	0	0	0	70.67	0
Pc	9	1246.5–1248.5	unknown	0	0	14.29	0	2.01	0	0	0	0	16.33	0
Pc	9	1270.5–1272.5	unknown	0	0	3.33	0	0	0	0	0	0	6.67	0
Pc	10	1289.5–1291.5	unknown	3.13	0	0	0	0	0	0	0	0	15.63	0
Pc	10	1313.5–1315.5	unknown	0	0	0	0	0	0	0	0	0	23.81	0

Note: BSPP, *Brigantedinium* species; BTEP, *Bitectatodinium tepikiense*; IACU, *Impagidinium aculeatum*; IMIC, *Islandinium ? Cezare*; IMIN, *Islandipagidinium* species; ISTR, *Impagidinium strialatum*; NLAB, *Nematosphaeropsis labyrinthus*; OCEN, *Operculodinium centrocarpum*; PARC, Cysts of *ratus*; PRET, *Pyxidinopsis reticulata*; PSCH, Cysts of *Polykrikos schwartzii*; SELO, *Spiniferites elongatus*; SFRI, *Spiniferites elongatus – Spiniferites frigiapplanatum*; TVAR, *Trinovantedinium variabile*.

SELO (%)	SRAM (%)	SFRI (%)	SSPP (%)	PDAL (%)	IMIN (%)	IMIC (%)	BSPP (%)	SNEP (%)	SQUA (%)	TAPP (%)	TVAR (%)	PSCH (%)	PARC (%)	PKOF (%)	PQUA (%)
1.44	1.44	0	0	37.41	12.95	0.72	10.79	0.72	0	0	0	0	0	0	0.72
2.74	0.68	0	0.68	27.40	22.60	0	19.86	0	2.05	0.68	0	0	0	0	1.37
1.05	2.11	0	0	13.68	13.68	2.11	49.47	0	2.11	0	0	0	0	0	0
0	0	0.94	0	27.36	24.53	0	23.58	0	0	0	0	0	0	0	0
2.78	0	0.69	0	25.00	16.67	0	27.78	0	0	0	0	0	0	0	0
3.36	0	0	0	16.78	26.17	0	30.87	0	0	0	0	0.67	0	0	0
2.56	1.28	0	0	23.50	29.91	0.43	24.79	0	0	0	0	0	0.43	0	0
0	2.60	0	0	28.57	31.17	0	12.99	0	0	0	0	0	0	0	0
4.87	1.77	1.77	0.88	9.29	14.16	0	10.18	0	0	0	0	0	0.88	0	0
3.21	0	0	0.0	5.77	28.85	1.28	14.74	0	0	0	0	0	0.64	0	0
4.22	0	2.27	0.32	8.77	13.64	0.65	6.49	0.32	0	0	0	0	0.97	0	0
6.67	0	0	0.0	2.67	16.00	0	2.67	0	0	0	1.33	0	0	0	0
5.10	1.02	0	1.02	6.12	27.55	1.02	24.49	0	0	0	0	0	0	0	1.02
0	0	0	0	3.33	63.33	0	16.67	0	0	0	0	0	0	0	6.67
0	3.13	0	0	28.13	21.88	0	25.00	0	0	0	0	3.13	0	0	0
0	0	0	4.76	19.05	28.57	0	23.81	0	0	0	0	0	0	0	0

nium minutum; IPAL, *Impagidinium pallidum*; IPAR, *Impagidinium paradoxum*; IPAT, *Impagidinium patulum*; ISPH, *Impagidinium sphaericum*; ISPP, *Im-Polykrikos* species – Arctic morphotype; PKOF, Cysts of *Polykrikos kofoidii*; PDAL, Cyst of *Pentapharsodinium dalei*; PQUA, Cysts of *Polykrikos quaddus*; SNEP, *Selenopemphix nephroides*; SQUA, *Selenopemphix quanta*; SRAM, *Spiniferitesramosus*; SSPP, *Spiniferites* species; TAPP, *Trinovantedinium*